Article:
Robrini, Ferial El, Amrouche, Badia, Cali, Umit et al. (2025) Assessment of machine and deep learning models integrated with variational mode decomposition for photovoltaic power forecasting using real-world data from the semi-arid region of Djelfa, Algeria. Energy Conversion and Management: X. 101108. ISSN: 2590-1745

https://doi.org/10.1016/j.ecmx.2025.101108

Energy Conversion and Management: X 27 (2025) 101108

Contents lists available at ScienceDirect

Energy Conversion and Management: X

journal homepage: www.sciencedirect.com/journal/energy-conversion-and-management-x

Assessment of machine and deep learning models integrated with variational mode decomposition for photovoltaic power forecasting using real-world data from the semi-arid region of Djelfa, Algeria

Ferial El Robrini [a,*], Badia Amrouche [a], Umit Cali [b,c,**], Taha Selim Ustun [d,*]

[a] Laboratory of Electrical Systems and Remote Control (LabSET), Renewable Energies Department, Faculty of Technology, Blida 1 University, 09000 Blida, Algeria
[b] Norwegian University of Science and Technology, Department of Electric Energy, O. S. Bragstads plass 2E, 7034 Trondheim, Norway
[c] University of York, School of Physics, Engineering and Technology, Heslington, York YO10 5DD, United Kingdom
[d] Fukushima Renewable Energy Institute, AIST, Japan

ARTICLE INFO

Keywords:
Grid-connected photovoltaic power plant
Long short-term memory
Deep learning
Prediction

ABSTRACT

Accurate photovoltaic power forecasting is essential for grid stability and efficient energy management. While Deep Learning (DL) and Machine Learning (ML) models are widely used, the extent to which each can be effectively leveraged remains an open question. This study thoroughly compares several ML and DL models, applied to both short-term (30-minute) and medium-term (3-hour) horizon. The research is built upon real-world data from a 53 MW PV plant located in Algeria, offering practical insights under realistic conditions. Another critical element of the study is the incorporation of Variational Mode Decomposition (VMD) for feature processing, which mainly enhances information extraction. The study also includes a monthly performance analysis investigating the climatological variability on forecasting accuracy. Among standalone models, CNN performs best with an nMAE of 2.9 %, nRMSE of 5.45 %, and R^2 of 0.9678 at 30 min ahead, and nMAE of 3.15 %, RMSE of 4.15 %, and R^2 of 0.9839 at 3 h forecasting. When combined with VMD, ML models, particularly ANN, SVM, and Random Forest frequently outperform DL-VMD counterparts. For instance, ANN achieves an nMAE of 1.08 %, nRMSE of 1.89 %, and R^2 of 0.9961 at 30 min, and maintains excellent accuracy at 3 h with nMAE of 1.1 %, nRMSE of 1.4 %, and R^2 of 0.9982. Collectively, this research serves as a reference for a multidimensional evaluation of forecasting performance. The analysis highlights the importance of selecting appropriate models and preprocessing techniques in PV power forecasting, tailored to location and climatological conditions, contributing to effectively addressing abrupt fluctuations and facilitating large-scale integration.

Introduction

Over the past few decades, renewable energy sources have become increasingly prominent in power supply systems, fueled by the rising demand for energy and their environmentally friendly attributes [1]. Renewables, particularly solar power, play a crucial role in decarbonizing sectors that are difficult to abate [2]. Supported by significant cost reductions, solar power has become the cheapest source of carbon–neutral energy worldwide [3], with further cost declines are anticipated, enabled by continuous technological advancements and the realization of economies of scale. [4]. Moreover, renewable energy possesses the potential to generate a broad spectrum of employment prospects across the entire value and supply chain. These opportunities span across procurement and production, sales and distribution, installation and connection, as well as operation, maintenance, and decommissioning [5,6].

Recent advancements in renewable energy utilization have been accompanied by improvements in the availability of power system data, including large-scale renewable energy generation and aggregate demand. The analysis of this data highlights the substantial repercussions of the inherent intermittency of renewable energy sources due to environmental conditions [7,8], which leads to various system faults [9] and affects multiple aspects of the power supply infrastructure, including voltage control, protection systems, frequency and angular stability of generators [10,11], harmonic management, and the overarching demands for flexibility and system stability [12,13]. This intermittency complicates the task of balancing real-time energy demand with grid

* Corresponding authors.
** Corresponding author at: Norwegian University of Science and Technology, Department of Electric Energy, O. S. Bragstads plass 2E, 7034 Trondheim, Norway.
E-mail addresses: elrobrini_ferial@univ-blida.dz (F.E. Robrini), umit.cali@ntnu.no (U. Cali), selim.ustun@aist.go.jp (T.S. Ustun).

https://doi.org/10.1016/j.ecmx.2025.101108
Received 25 April 2025; Received in revised form 13 June 2025; Accepted 14 June 2025
Available online 19 June 2025

Nomenclature

ADMM	Alternating Direction Method of Multipliers
ARMA	AutoRegressive Moving Average
ARIMA	AutoRegressive integrated Moving Average
BiLSTM	Bidirectional Long Short-Term Memory
BMO	Barnacle Mating Optimization
CARDS	Coupled AutoRegressive with Dynamic System
CEEMDAN	Complete Ensemble Empirical Mode Decomposition with Adaptive Noise
CFNN	Cascade-Forward Neural Network
CNN	Convolutional Neural Networks
ConvLSTM	Convolutional LSTM
DL	Deep Learning
ELM	Extrem Learning Machine
FFNN	Feed-Forward Neural Network
EMD	Empirical Mode Decomposition
GA	Genetic Algorithm
GBR	Gradient Boosting Regressor
GHI	Global Horizontal Irradiance (W/M^2)
GNI	Direct Normal Irradiance (W/M^2)
GRNN	General Regression Neural Network
GRU	Gated Regression Unit
GSA	Grid Search Algorithm
GSR	Global Solar Irradiance (W/M^2)
IAMFN	Inception-Embedded Attention Memory Fully-Connected Network
IEDN	Inception Embedded Deep Neural Network
IEDN-RNET	Inception Embedded Deep Neural Network with Resnet
IF	Terative Filtering Decomposition Method
IMF	Intrinsic Mode Functions
LR	Linear Regression
LSTM	Long Short-Term Memory
LM	Levenberg-Marquardt
MAE	Mean Absolute Error
ML	Machine Learning
MLR	Multiple Linear Regression
MWSO	Modified White Shark Optimization Algorithm
NARX	Non-Linear Autoregressive Neural Network with Exogenous Inputs
NSE	Nash-Sutcliffe model efficiency coefficient
nRMSE	Normalized Root Mean Square Error
OP	Operating System
PCA	Principal Component Analysis
PDPP	Partial Daily Pattern Prediction
PL	Power-Law
P_{PV}	Output Power (Kw)
PV	Photovoltaic
r	Coefficient of correlation
R^2	Coefficient of Determination
RBFN	Radial Basis Function Neural Network
RBM	Restricted Boltzmann Machine
RE	Relative Error
Resnet	Residual Networks
RNN	Recurrent Neural Networks
RMU	Ring Main Unit
SAE	Stacked Auto Encoders
SARIMA	Seasonal ARIMA
Time2Vec	Time to vector
TCM	Time Correlation Modification
TVF	Time Varying Filter
UPS	Unit Power System
USPVPS	Utility Scale PhotoVoltaic Power Systems
VAEs	Variational AutoEncoders
VMD	Variational Mode Decomposition

production [5,14]. As a result, the effective integration of photovoltaic generation into energy systems depends on the ability to accurately anticipate and manage fluctuations [13,15,16]. Central to this process are accurate load and power forecasting, which are critical components of the Energy Management System (EMS). The EMS guides operational choices in power grids, ensuring optimal management of energy supply and demand between producers and load [17,18]. By enabling such precision, effective energy management can reduce electricity costs by approximately 20–30 %[19].

The prediction of photovoltaic generation involves estimating the future energy output of a specific PV station based on diverse elements, including spatial and temporal resolution [20,21], geographic location, weather conditions, seasonal changes, solar panel performance, power plant surface, and additional data related to photovoltaic energy exploration [22]. Predictions are generated by analyzing historical data, identifying trends and patterns, specifying correlations, and extrapolating this information to create accurate projections and forecasts. Several methods for forecasting PV production are documented in the literature. Comprehensive evaluations of the latest advancements in the field can be found in various sources [23–29]. Numerous PV power prediction models have been introduced, all aiming to achieve better forecast accuracy with less computational cost [30]. These models are mainly classified based on the predictive model type and architecture, which can be categorized into persistence or naïve predictors [31–33], physical techniques such as cloud-based models and Numerical Weather Predictors [30,34], statistical techniques including empirical methods such as ARMA, ARIMA [35,36], SARIMA [36,37] and CARDS [38], machine learning-based (ML) and Deep Leaning models (DL) such as Artificial Neural Networks [39–44], Support Vector Machine [45–47], Genetic Algorithms [48], Random forest [49], Boosted Decision Tree [50], c-means, and k-means [51], and Expert Systems [42,51–54]. Additionally, there are ensemble or hybrid models that reunite two or more predictive models to benefit from the best features of each [36,50,55].

Another categorization found in existing literature involves the temporal prediction horizon, which delineates the intervals at which forecasts are generated. Forecasts for PV energy can span diverse timeframes, encompassing long, medium, short, and very short-term forecasts. The temporal precision is contingent upon the particular requirements and purposes of the forecast, whether it be optimizing energy administration or strategizing for grid incorporation. A third classification approach is based on data type and category, depending on training/testing data variety, which ultimately affects the predictive accuracy [30]. For example, the meticulous selection of pertinent and accurate input data is imperative to attaining precise outcomes. Erroneously selecting pivotal, impactful variables will inevitably increase the margin of prediction error, as approved in [47,56]. An overview of the classification methodologies is represented in Fig. 1:

Related work

During the last decades, numerous studies have been published on forecasting photovoltaic generation that exhibit significant differences, mainly due to the varied input datasets they utilize, including photovoltaic data, solar irradiation, temperature, air pressure, humidity, wind direction, and speed. Furthermore, these approaches vary in their forecasting horizons, techniques, and algorithms [57]. Nowadays, hybrid methodologies that combine different types of models have

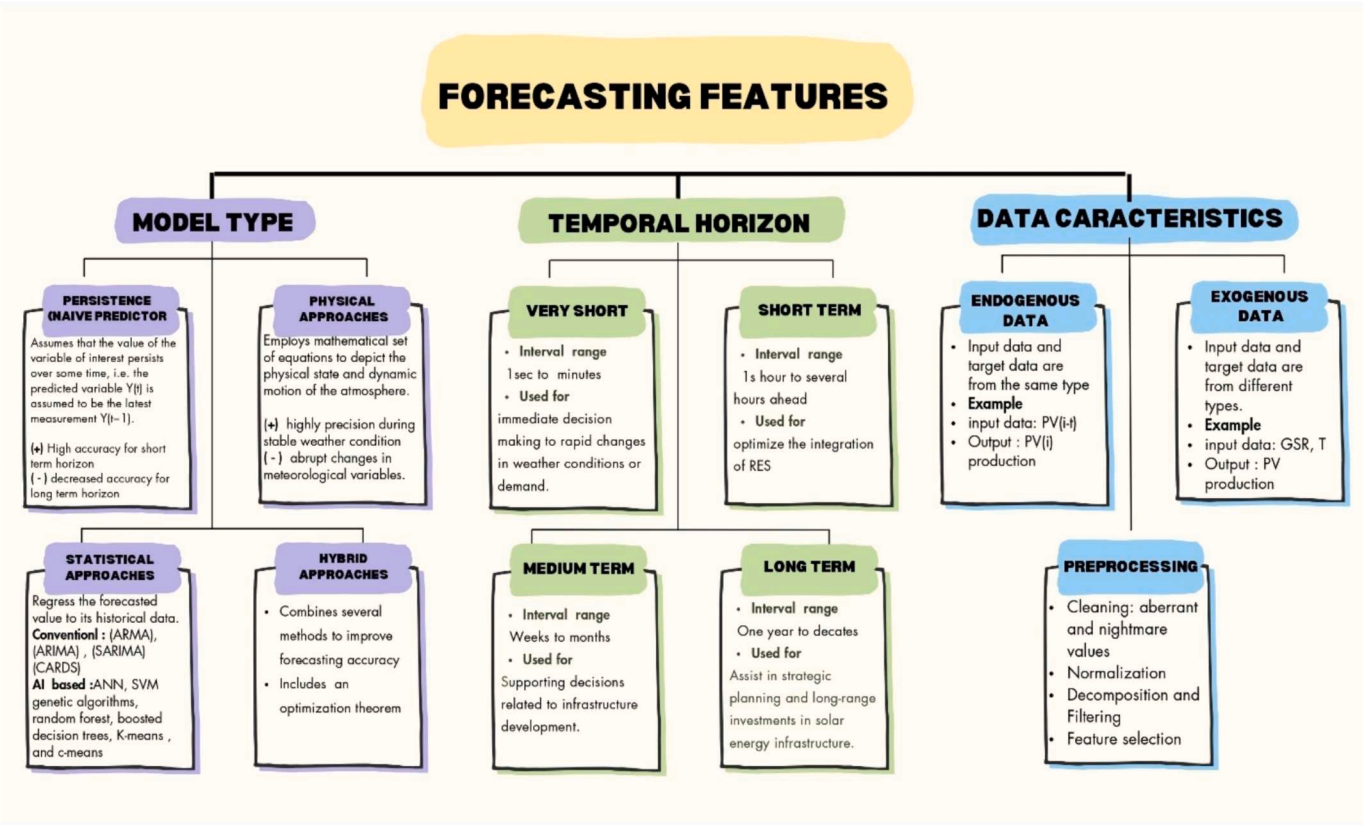

Fig. 1. Classification of the forecasting methodologies.

proven to be effective solutions for improving prediction performance.

In the work of Gang et al. [58] a hybrid forecasting model is developed for photovoltaic and wind power generation. This model incorporates a Time2Vec embedding layer for data preprocessing, a CNN With a Wider first layer kernel (WDCNN) for feature extraction, as well as a BiLSTM network for predictive modeling. The Time2Vec layer plays a pivotal role in simplifying the input data preprocessing by partitioning the time series data into both aperiodic and periodic components. The study of Feroz Mirza et al. [59] introduced an IEDN-RNET model, combining Inception modules with various kernel sizes for capturing diverse abstraction levels, ResNet blocks for addressing gradient vanishing issues and capturing local and global patterns, Bidirectional weighted LSTM and GRU layers for handling sequential data's long-term interrelations and dynamics from past and forthcoming information simultaneously, and Time2Vec method for capturing periodic patterns. Wang et al. [60] developed an LSTM-RNN-based model for day-ahead PV power forecasting to address the issue of PV power fluctuations using data from the previous day. Subsequently, the TCM principle is used to adjust the LSTM-RNN output model based on trends and regularities observed in historical data from previous years.

Nature-inspired *meta*-heuristic algorithms exhibit significant potential for addressing optimization problems. The adaptability of these algorithms is closely linked to their tuning factors. The WSOA has been employed as a standard optimization technique, effectively addressing control applications without substantial modification to its tuning parameters. The WS is a top-tier predator and a highly agile navigator, possessing a streamlined physique that enables rapid tracking of its targets. Numerous attributes underlie the excellence of WS behavior in nature as an optimization process, primarily pertaining to its ability to track, explore, and search for prey in close proximity. Mansoor et al. [61] suggested two new hybrid models using a MWSO-GRNN and MWSO-RBFN for short-term wind power forecasting. Seasonal findings are systematically analyzed both visually and analytically, employing 15 min ahead forecasting with four hybrid artificial neural network architectures in amalgamation with PSO and BMO stochastic optimization algorithms that are respectively: PSO-RBFN, PSO-GRNN, BMO-RBFN, and BMO-GRNN. Hassan et al. [62], implemented a hybrid model grounded on a NARX model and utilized GA for gradient-free training. Through an evaluation of the NARX-GA models at various time horizons and several Algerian and Australian regions, the study found that these models provide highly accurate estimates.

In Algeria, Kedouda et al. [63] explored the utilization of a Feed-Forward Neural Network (FFNN) along with two regressive models: RPL and PL. The objective was to predict the output of a 160 W PV module location in El-Oued, Algeria, trained on a dataset encompassing six days of experimental data (172,800 × 7 data points). The study identified solar radiation, ambient temperature, and module temperature as key factors strongly correlated with PV power generation. Notably, the LM algorithm delivered the best results for training the ANN model. Khelifi et al. [64] analyzed the implementation of a TVF-EMD and an ELM model. The developed TVF-EMD-ELM methodology has been validated for forecasting up to a maximum horizon of 30 min and has been evaluated and verified on four separate Algerian PV power datasets with varying climate conditions. Guermoui et al [65] conceived a novel integrated structure based on the Recursive Intrinsic Functions decomposition technique and ELM. The methodology is adjusted for a maximum forecasting horizon of 60 min. PV power data was disassembled into various IMFs functions via the IF method, transitioning from higher to lower frequencies. Subsequently, the IMFs are feed to the ELM forecasting model to generate the desired PV power output.

Ziane et al. [66], explored the interdependencies between the meteorological parameters and the generation of the grid-connected PV station of Zawiet Kounta (Adrar). Feature selection and PCA analysis were employed as techniques for dimensionality reduction and preprocessing of input data before training random forest models. VAEs are powerful unsupervised generative techniques known for automatically

extracting information from data. They excel at dimensionality reduction, compressing high-dimensional data effectively. VAEs also approximate complex data distributions efficiently through stochastic gradient descent. They mitigate overfitting issues through built-in regularization during training, making them effective for diverse applications involving complex data. Dairi et al. [67] provided a VAE for single- and multi-step-ahead forecasting of a 9 MW grid-connected PV power plant in Timimoune. The results highlight the strong performance of deep learning techniques in solar power forecasting, with the VAE consistently outperforming other methods.

Main contribution

The deployment of ML, DL, and hybrid approaches in PV forecasting has been both prolific and innovative in recent years. While this methodological diversity reflects the field's dynamism, it also introduces complexity and ambiguity for grid operators who must select models tailored to their operational constraints, regional data availability, and unique climatological characteristics. Against this backdrop, the present research proposes a structured evaluation of PV power forecasting models, designed to provide a decision-support framework and facilitate the seamless integration of large-scale PV power into the energy mix. The contribution is articulated through several key components, each addressing a critical aspect of effective PV forecasting and integration:

- **Real-World Application:** The study is grounded in empirical data collected from a 53 MW PV power plant located in Djelfa, Algeria; a region characterized by a semi-arid climate. This setting provides a realistic and practical testbed for evaluating model performance under real-world conditions.
- **ML and DL Model assessment:** To analyze the PV plant data effectively, A broad suite of ML and DL models is rigorously evaluated. LSTM and GRU are tailored for capturing long-range dependencies in time-series data, with GRU providing a more computationally efficient architecture. Their bidirectional extensions (BiLSTM, BiGRU) enhance temporal representation by incorporating both past and future contextual information. ANN is employed as a baseline model, underscoring the gains achieved by more sophisticated architectures. SVM seeks the optimal hyperplane that maximizes margin, ensuring robust generalization in high-dimensional feature spaces. RF, as an ensemble technique, improves prediction stability by aggregating multiple decision trees. CNNs are leveraged to extract spatial features, capturing local dependencies within the PV dataset. ResNet introduces residual connections that alleviate vanishing gradient issues, facilitating deeper and more stable networks. Meanwhile, the Inception architecture enriches feature extraction by applying multi-scale convolutions in parallel, increasing representational capacity without excessive depth.
- **Dual Forecasting Horizons:** The analysis encompasses two forecasting horizons: short-term (30 min ahead) and medium-term (3 h ahead), thereby offering insights into both immediate and near-future grid operational planning.
- **Hybridization with VMD:** The research investigates the integration of VMD as a preprocessing step to enhance the predictive capabilities of ML and DL models, addressing the non-stationary nature of solar power signals.
- **Monthly Performance Evaluation:** A granular, month-by-month assessment is conducted to explore the influence of climatological variability on model accuracy, thereby emphasizing the seasonal dynamics that affect forecast reliability.
- **Contextualized Insights:** The findings underscore the critical role of local weather fluctuations in determining forecasting precision. They highlight the necessity of selecting both appropriate predictive models and preprocessing strategies that are specifically adapted to regional climatic conditions and data characteristics.

Through this multi-faceted approach, the study contributes a robust and context-aware framework for PV power forecasting. By aligning advanced predictive techniques with local operational realities, it supports grid operators in navigating the complexities of PV integration, ensuring system stability, and ultimately advancing the deployment of renewable energy on a larger scale.

Material and methods

Characteristics of weather in Djelfa

Understanding the local climate in Djelfa is essential due to its significant impact on performance studies. Located approximately 300 km south of Algiers, at coordinates 34°40′N latitude and 3°15′E longitude, Djelfa sits at an average altitude of 1,110 m above sea level. The region covers an area of 542.2 km^2 and is characterized by semi-arid conditions, marked by considerable temperature variations, low annual precipitation, and high solar irradiance levels [68]. Djelfa experiences seasonal fluctuations, frequent weather variability, and a predominance of clear skies throughout most of the year. These climatic conditions provide a unique environment for evaluating the robustness of predictive algorithms.

According to the World Meteorological Organization [69], the temperature extremes in Djelfa exhibits significant variation. Daytime highs range dramatically from a relatively cool 9.8 °C to a peak of 33.8 °C, with the highest temperatures typically recorded during the summer months. In contrast, the minimum temperatures follow a similar seasonal fluctuation, starting at a chilly 0.1 °C in the winter and rising to a more temperate 18.3 °C during the warmer summer months. Fig. 2 illustrates the variation in daylight hours and temperature patterns throughout the year in Djelfa [70]. The duration of daylight fluctuates moderately, with solar exposure ranging from 10.1 to 14.5 h per day. This variability results in daily sunshine durations ranging from 6.8 to 12 h, ensuring a substantial amount of sunlight during the year.Fig. 3..

The relative humidity in Djelfa fluctuates between 24 % and 65 %, reflecting the region's semi-arid climate. The city receives annual rainfall ranging from 8 mm to 34 mm, with the driest month experiencing very minimal precipitation. Wind speeds reach their peak in March, averaging 19 km/h, while August is the calmest month, with wind speeds decreasing to 12.4 km/h. Cloud cover is most extensive in January, reaching 31 %, whereas June experiences the least cloud cover at just 11 % [70].

The studied PV systems

This study uses a dataset comprising one grid-connected photovoltaic (PV) station. The power station modules technology is polycrystalline silicon, generating a total capacity of 53 MW and covering an area of 120 ha. The schematic diagram and main components of the studied power station, as well as its main specifications are represented in Fig. 4 and Table 1, respectively. Additional figures and detailed descriptions related to the power station are available in the authors' previous works [71,72].Table 2..

Data analysis

Generally, the evolution of daily photovoltaic generation is characterized by a gradual rise in the morning, a peak during midday, and a gradual decrease towards sunset. Although this pattern is a standard representation of PV generation behavior, it is only meaningful on sunny or clear sky index days. However, highly irregular (intermittent) patterns are observed when other meteorological conditions are identified, such as variable clouds, rain, snow, or sandstorms. Fig. 5 provides various representations of the daily generation of PV.

Throughout the year, PV power energy fluctuates due to solar radiation variations. These divergences are primarily influenced by the

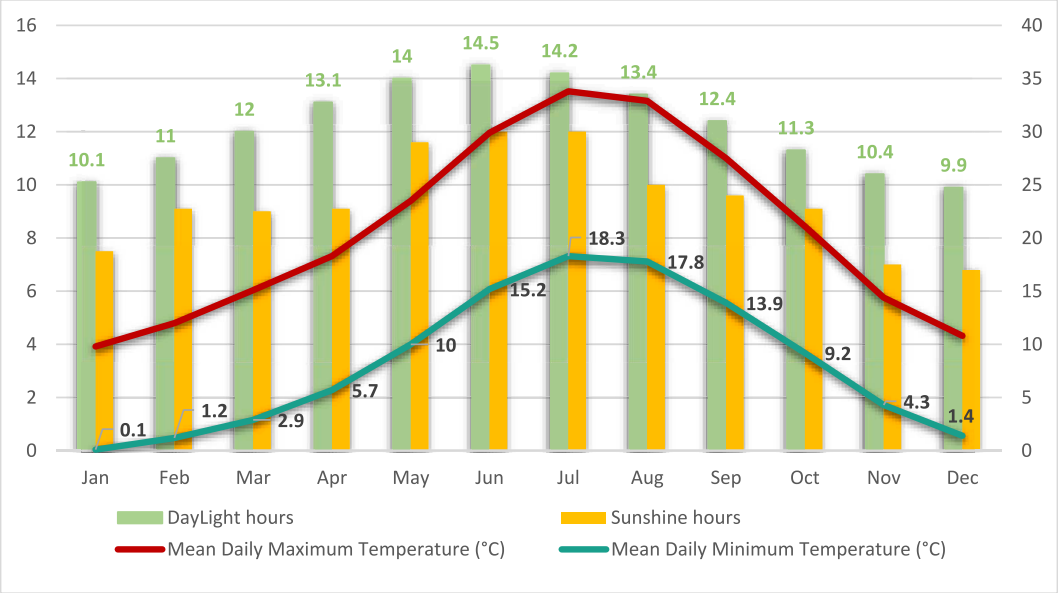

Fig. 2. Climatic Characteristics of Djelfa Region: Sunshine, Daylight, Max and Min daily Temperatures (1976–2005).

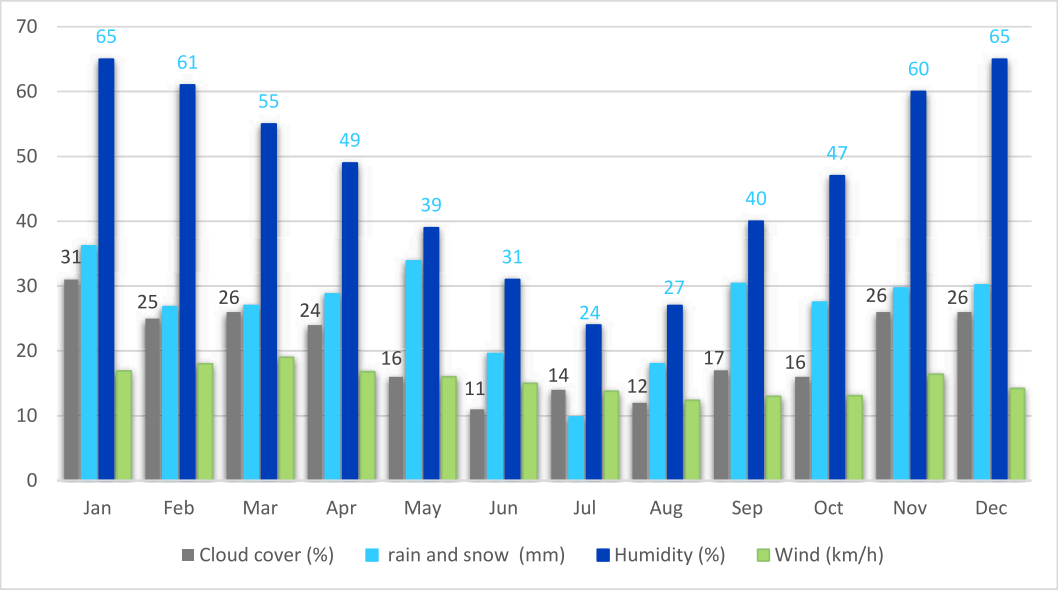

Fig. 3. Climatic Characteristics of Djelfa Region: Cloud Cover, Precipitation, Humidity, and Wind Speed.

Earth's elliptical trajectory encircling the Sun, which changes the distance between the Earth and the Sun, and thereby the tilt of the Sun's rays, known as the solar incidence angle. This variation impacts the intensity of solar radiation received and thereby the potential of PV generation. Table 3 offers a statistical analysis of the generated power for the studied PV farm, showing various values produced over the months, with the Spring season remaining the best season for the studied PV farm as the maximum produced PV is attained on February, ten at 14 h:00 ($maxP_{max} = 58.34$ MW). Moreover, the maximum value of Pmax is recorded during March ($meanP_{max} = 46.42$ MW). While a decline in maximum production is registered during warm months such as August, July, and June. Finally, the minimum value of P_{max} is obtained on November, 24th at 15 h:00 ($minP_{max} = 7.41$ MW).

Investigated predictive models

Long Short-Term memory Networks

The LSTM model, a specialized category of RNN, is distinguished by its unique architecture, which includes weighted connections, memory retention capabilities, and feedback mechanisms. A central component of the LSTM is the memory cell (MC), which serves as persistent storage throughout the network's computations. This memory cell enables the transfer and preservation of information across the sequence, with the flow of data regulated by a series of gate mechanisms. Unlike traditional RNNs, LSTM is adept at retaining important information over long sequences, effectively addressing the vanishing gradient problem that hampers standard RNNs. [73 74]. LSTM architecture involves adding three gate structures: input, output, and forget gates. Forget Gate assists in eliminating redundant information and retaining only the relevant information to proceed with prediction [75]. The input gate (i_t) controls

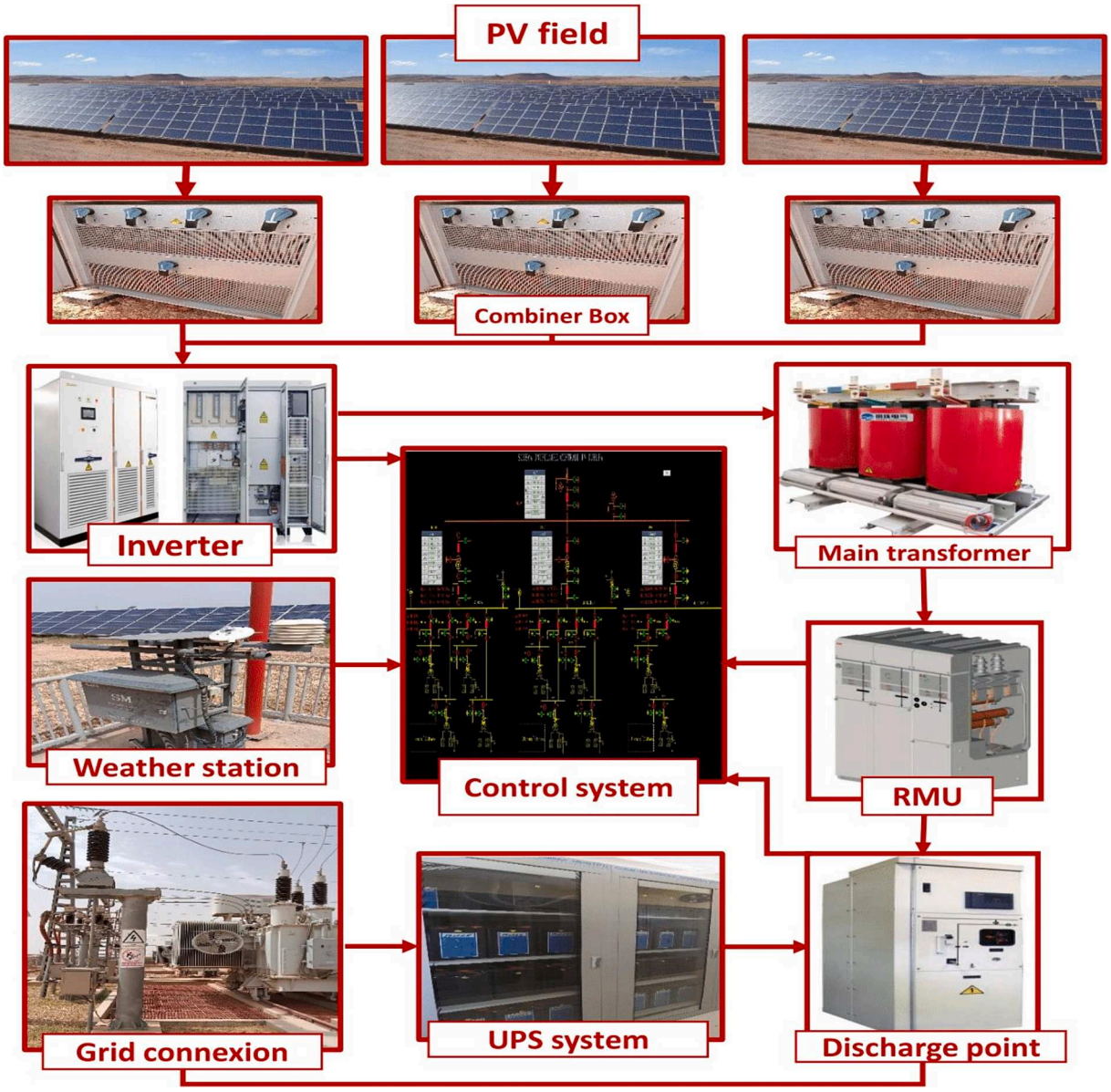

Fig. 4. Schematic diagram and main components of the studied power station.

Table 1
Main specifications of Djelfa PV plant.

Specifications			
Total Capacity (MW)	53	Module reference	YL250P-29b
Module technology	Polycrystalline	Total N° of panels	212212
N° subfields	53	N° of panels/field	4004
N° of transformers	53	N° of combiner boxes/ field	24
N° of inverters	53		

the flow of new information and indicates if, and to what degree new information should be incorporated in the current state cell (c_t). The output gate (o_t) regulates the amount of information carried forward from the last time step to the forward, in conjunction with the data from the current time step [76]. The computed metrics are in the 0 to 1 forget gate scale. When the f_t is close to 1 and the i_t is close to 0, LSTM can maintain long-term memory. Conversely, when these values differ, the network facilitates short-term memory [73,74].

The mathematical formulations used in the LSTM network are the following: [74,76–78].

To calculate the gate units

$$i_t = \sigma(W_i x_t + U_i h_{t-1} + b_i) \quad (1)$$

$$f_t = \sigma(W_f x_t + U_f h_{t-1} + b_f) \quad (2)$$

$$o_t = \sigma(W_o x_t + U_o h_{t-1} + b_o) \quad (3)$$

To update the memory unit

$$\bar{c}_t = tanh(W_c x_t + U_c h_{t-1}) \quad (4)$$

$$c_t = f_c{}^* c_{t-1} + i_t{}^* \bar{c}_{t-1} \quad (5)$$

To calculate the output of the LSTM unit:

$$h_t = o_t{}^* tanh(c_t) \quad (6)$$

The cell state of the MC is denoted c_t, and the candidate MC is expressed as $\bar{c}_t$, where c_{t-1} represents the cell state at time t_{-1}. Additionally, x_t denotes the input components, and h_t Corresponds to the hidden state. W_{ix}, W_{fx}, W_{ox}, and W_c are the weights for the i_t, f_t, o_t, and $\bar{c}_t$,

Table 2
Monthly variation of Maximum and Mean PV power.

Month		*01*	*02*	***03***	*04*	*05*	*0*	*07*	*08*	*09*	*10*	*11*	*12*
P_{max}	***Mean***	*41.58*	*40.31*	***46.42***	*41.62*	*41.81*	*38.78*	*37.67*	*40.00*	*39.9*	*41.78*	*39.73*	*41.99*
	Max	*47.23*	***58.34***	*56.50*	*55.50*	*47.72*	*43.24*	*40.73*	*48.11*	*45.4*	*49.47*	*48.37*	*47.14*
	Date	*01st*	***10 st***	*20 st*	*11 st*	*01 st*	*07 st*	*09 st*	*10 st*	*27 st*	*29 st*	*14 st*	*28 st*
	Time	*12:30*	***14:00***	*13:00*	*12:30*	*12:00*	*12:30*	*12:30*	*13:30*	*13:30*	*12:30*	*13:00*	*13:30*
	Min	*16.21*	*14.15*	*36.1*	*15.59*	*29.68*	*23.27*	*33.77*	*12.26*	*32.08*	*18.96*	***7.41***	*39.72*
	Date	*19 st*	*08st 16:00*	*08 st*	*03 st*	*19 st*	*24 st*	*28 st*	*12 st*	*09 st*	*28 st*	***24 st***	*08 st*
	Time	*13:00*		*14:30*	*17:30*	*12:30*	*12:30*	*12:30*	*14:00*	*13:00*	*13:30*	***15:00***	*14:00*
P_{mean}	***Mean***	*16.43*	*15.44*	*17.64*	*18.19*	*18.23*	***19.88***	*18.37*	*18.17*	*16.76*	*16.96*	*14.90*	*17.01*
	Max	*20.24*	*24.01*	*24.14*	***24.17***	*24.16*	*23.14*	*20.62*	*22.50*	*22.22*	*22.41*	*21.58*	*18.74*
	Date	*23 st*	*25 st*	*27 st*	***05 st***	*02nd*	*06 st*	*30 st*	*04 st*	*28 st*	*18 st*	*04 st*	*31 st*
	Min	*4.99*	*5.23*	*10.53*	*3.41*	*9.78*	*14.61*	*15.41*	*4.38*	*6.93*	*4.01*	***2.05***	*16.69*
	Date	*19 st*	*21 st*	*24 st*	*17 st*	*19 st*	*01 st*	*08 st*	*12 st*	*09 st*	*16 st*	***24 st***	*21 st*

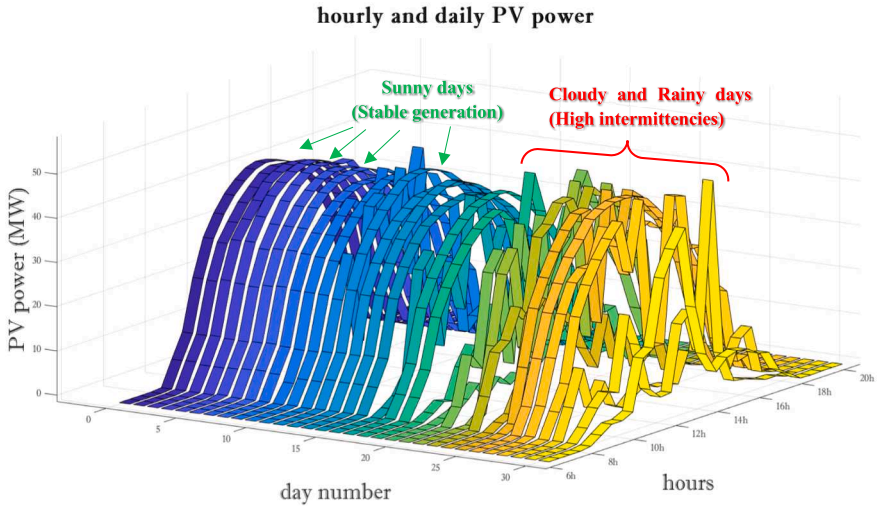

Fig. 5. Hourly and daily PV power output.

respectively. W_{ih}, W_{fh}, W_{oh} , and $W_{\tilde{c}_t h}$ represent the hidden layer's weight matrices. Subsequently, W_{ic}, W_{fc}, W_{oc} are weight matrices for the candidate cell state. Subsequently, b_i, b_f, b_o, and b_g stand for the bias vectors associated with the three gates and MC, respectively. The activation function utilized includes the sigmoid function (σ) and the hyperbolic tangent function (tanh). In an NN, the activation function serves as a mathematical operation associated with a node (or neuron) that is activated when the input value of the node contributes significantly to the prediction process. Numerous categories of activation functions exist, with hyperbolic tangent, sigmoid, and logistic functions being the most utilized [79].

Gated Recurrent Unit

Unlike the LSTM, which uses three gates, the GRU simplifies its design by fusing the input and the forget gates into a unified update gate. As a result, the GRU relies on just two gates called: the update gate and the reset gate. The reset gate controls how much of the previous hidden state should be discarded, while the update gate governs how much of the new input should be integrated into the hidden state. This hidden state is then adjusted based on the reset gate, update gate, and the current input. The streamlined GRU architecture enhances convergence speed and helps mitigate the gradient issues encountered in RNNs. [80]. The inner structure of the GRU is represented by the equations (7–10), Where h_{t-1} is the transmitted state from the previous cell, x_t denotes the current node's input, h_t signifies the hidden layer output, r_t refers to the reset gate, z_t represents the update gate, $\tilde{h}_t$ Is the candidate's hidden state, and (1-) symbolizes the data forwarded by the link as 1-z_t. The sigmoid function facilitates the transformation of data into a scale between 0 and 1, thereby serving as a gating mechanism. As r_t nears zero, the selectivity of the model retains exclusively the present input information while discarding previously held hidden information. Conversely, as r_t approaches to 1, the model preserves historical information. The value of z_t varies from 0 to 1; higher values of the gated signal imply greater retention of information.

The units derived from GRU can be computed using the following equations [80]:

- Reset gate

$$r_t = \sigma(W_{rx}x_t + W_{rh}h_{t-1} + b_r) \tag{7}$$

- Update gate

$$z_t = \sigma(W_{zx}x_t + W_{zh}h_{t-1} + b_z) \tag{8}$$

- Candidate hidden state

$$\tilde{h}_t = tanh(W_{hx}x_t + r_t \odot (W_{hh}h_{t-1}) + b_h) \tag{9}$$

- New hidden state

$$h_t = (1 - z_t) \odot h_{t-1} + z_t \odot \tilde{h}_t \tag{10}$$

Table 3
Hyperparameter tuning step.

Model	Hyperparameter range	Best preferences
ANN	Neurons number per layer: [10,20,30] Hidden layers number: [1–3] Training algorithm: Levenberg-Marquardt Architecture: Feed Forward Hidden Layer activation function: ReLu Output layer: Linear	Neurons number = 10; Hidden layers number = 1
SVM	Kernel type: RBF C values: [0.1, 1, 10] Sigma values: [0.1, 1, 10]	C values = 0.1 Sigma values = 1
RF	Function: Tree Bagger Num. of Trees = [100, 200, 300]; Min. Leaf Size = [1,5,10]; Method: Regression k-folds = 5	Num. of Trees = 300; Min. Leaf Size = 10;
LSTM/ BiLSTM	Hidden Unit = [50, 100, 150, 200] Epochs grid = [50, 100, 200] training algorithm: adam Dropout: 0.2 Size of Mini Batch: 64 Initial Learning Rate: 0.01	Hidden Unit = 200 Max Epochs: 100
GRU/BiGRU	Hidden Unit = [50, 100, 150, 200] Epochs grid = [50, 100, 200] training algorithm: adam Size of Mini Batch: 64 Initial Learn Rate: 0.01 GruLayer: 1	

Bidirectional Recurrent Networks

In photovoltaic PV power forecasting using time series data, it is crucial to carefully account for the influence of both historical and future values on the present value to ensure accurate predictions. To this end, constructing forward and backward RNN models proves advantageous for capturing the complex dependencies between preceding and subsequent factors affecting the forecast. Bidirectional Recurrent Neural Networks (BiRNNs), such as BiLSTM or BiGRU, contain two hidden layers that operate in opposite directions, producing a unified output. The data is processed in two temporal sequences: one following the traditional forward order and the other in reverse. This bidirectional approach allows the model to incorporate information from both prior and future time steps at every instance. It is essential to highlight that while bidirectional neurons function independently during the forward and backward passes, only the weights are updated during training.

$\{x_{t-1}, x_t, xt_{+1}\ldots. x_n\}$ are the signal's input, whereas $\{h_{t-1}, h_t, h_{t+1}\ldots. h_n\}$ denotes the network's output. To calculate y_t prediction at time t, the following activation function is used: [79]

$$y_t = f\left(W_y\left[\overrightarrow{h_t}; \overleftarrow{h_t}\right] + b_y\right) \tag{11}$$

W_y: is the network's final transformation weight based on the input and volume set. $\overrightarrow{h_t}$ and $\overleftarrow{h_t}$ Represent the forward hidden state and the backward hidden state, respectively. $\left[\overrightarrow{h_t}; \overleftarrow{h_t}\right]$ Refers to the concatenated hidden state. b_y The bias vector is associated with the final transformation layer.

Forecasts for PV power frequently span hours, if not days, making the method's adeptness in capturing extended dependencies exceedingly valuable. By accounting for both historical and future time increments, the model produces dependable forecasts for extended durations. The Bidirectional mechanism empowers the model to grasp temporal trends, manage periodicity, depict time-based correlations, and enable precise long-term predictions. Integration of these temporal features notably augments the precision and dependability of PV power prediction, thereby fostering progress within the domain [59].

Support vector Regressor Machine

SVMs primarily serve as classification algorithms that distinguish data points into two distinct categories using hyperplanes in a higher-dimensional space. SVMs aim for optimal separation by choosing the hyperplane that maximizes the margin [81], defined as the shortest distance between the hyperplane and the closest data points in each category. SVR extends SVMs to predict continuous values, maintaining the principles of maximizing the margin and the use of the kernel trick. [82]. SVR function is defined by [83]:

$$f(x) = w^T \cdot \varphi(x) + b \tag{12}$$

Where $\varphi(x)$ represents the Kernel function, x the feature vector input, w^T The transpose of the weight vector w. b the bias term or intercept, and $f(x)$ being the target output.

In SVR, the kernel function specifies how input data is transformed into an elevated-dimensional feature space. This transformation enables the capture of nonlinear relationships linking the input features to the dependent variable. There are primarily three types of kernel functions [82,84,85]; linear, polynomial, and radial basis function (RBF). Thorough a preliminary study, RBF is chosen in this research, whose equation is given below:

$$k(x, xi) = exp\left(-\gamma \|x - x_i\|^2\right) \tag{13}$$

$\gamma = \frac{1}{2\sigma^2}$: represents the Kernel coefficient or the regularization parameter; smaller values result in a broader neighborhood being considered similar, whereas larger values concentrate on points that are closer to each other. σ represents the tuning parameter.

Random Forest

RF regression is defined as an ensemble learning technique utilized for regression tasks, including forecasting PV power generation. It operates by constructing multiple decision trees during training and generating the average of each tree. Each final node in a tree is assigned a response (R_i) determined by the predominant category for classification; otherwise, by the mean value for regression. The prediction $T_i(X)$ is given by [86,87]:

$$T_i(X) = R_i \tag{14}$$

The minimizing algorithm aiming to decrease variance while preserving low bias is given by:

$$\mathrm{MSE(D)} = \frac{1}{|D|}\sum_{i \in D}(y_i - \bar{y}_d)^2 \tag{15}$$

Where $|D|$ is the instance number in node D. y_i: Is the value of the target for instance I. $\bar{y}_d$: Is the average target value.

Convolutional Neural Networks

CNNs are stimulated by the human brain object identification mechanism. Two-dimensional CNNs excel in computer vision tasks such as facial recognition, image classification, natural language processing, and handwriting applications [88]. Additionally, one-dimensional CNNs are also employed in regression applications by exploiting their automatic feature extraction [89,90]. For PV power forecasting, CNNs are widely used to obtain the spatial features contained within the PV dataset. A basic CNN entails an input, a convolutional, a pooling, and an output layer [91]. The convolutional layer of CNN serves as a spatial feature extraction layer, which incorporates a novel feature derived from the input data for every timestamp by computing the dot products between the input and the sliding convolutional kernel across the width and height [92]. For multivariate time series, the slide across height is insignificant due to fewer connections amidst different variables within the same sequence location. Therefore, a 1-D convolution kernel, sliding across only the sequence dimension, is used [93], and the output is defined by:

$$y = x^{*}w, y[i] = \sum_{k=-\infty}^{+\infty} x[i+k]\, w[k] \tag{16}$$

With x defined as the input vector, and ω refers to a filter or kernel.

The fundamental idea behind contemporary DL techniques is that enhancing the number of convolutional layers leads to better overall performance by enriching the high-level feature extraction [94,95]. Training deep NNs can present several challenges. One significant issue is the vanishing gradient problem, which occurs when gradients back-propagate through earlier layers. Furthermore, repeated accumulation can lead to gradients diminishing to an exceedingly small value, which leads to overfitting and causes network degradation [94,96]. It is within this context that Residual and inception modules are introduced to put forward to solve this problem.

Residual modules: In 2016, Kaiming et al.[97] first introduced the fundamental notions of a Residual Network (ResNet). The concept involves implementing a shortcut connection that permits the earlier output layer to be directly passed as input to the subsequent layer without any modifications. Residual connections between layers enhance the flow of information and are used to transmit important features to deeper layers. This facilitates the effective combination of feature maps, leading to stronger predictions [98]. They can also serve to speed up the convergence and shorten the training time [95] The shortcut modules utilized in ResNet, encompass two types: the Identity block, which lacks a convolution layer in the shortcut and maintains equal dimensions for the input and output flow, and the Convolutional block, which features a convolution layer with batch normalization incorporated into the shortcut. Following the block design, as soon as the residual mapping is coming close to zero, the block directly performs the identity mapping, as the residual mapping approaches zero, the block resorts solely to identity mapping. This approach safeguards the original information through establishing a direct shortcut bridge linking the input to the final output. Consequently, this strategy plays a crucial role in reducing any decline in network performance [99], and the learning difficulties are simplified [94]. In practical implementation, the residual mapping is commonly not zero, enabling the block to effectively learn and adjust the residuals [94,100]. As a residual form, the original mapping may be written as follows:

$$f(x) = h(x) - x \tag{17}$$

where h(x) is the original mapping, x is the input feature, and f is the residual function. Thus, the original mapping can be reformed as F(x) + x.

Inception modules: The Inception network architecture allows the use of filters with different sizes without increasing the network's depth, challenging the typical approach of adding more convolutional layers to enhance performance in most CNN variants [95]. The inception module is recognized for its capacity to gather features at multiple scales and accommodate different sizes of receptive fields, and is it specifically selected to complement and improve the performance of CNN. In an inception module, the different filters are added parallelly instead of being fully connected one after the other [59,95]. The original inception block comprises three, each utilizing distinct kernels for feature extraction. This configuration block helps to augment robustness and significantly enhance feature extraction in time series [101]. In this paper, the Inception V1 is applied.

Variational Mode Decomposition

To conduct an in-depth analysis of PV power fluctuations, it is essential to decompose the time series data into simpler, more interpretable components [102]. In 2014, Dragomiretskiy and Zosso developed an innovative method so-called VMD [103], that offers a sophisticated approach tailored for analyzing nonstationary and nonlinear time series data. VMD leverages an ADMM to enhance the decomposition process, thus improving its accuracy and robustness in signal analysis. In applying VMD, the time series data f(t) is partitioned into (K) intrinsic mode functions $u_{(k)}$. Every k(t) is associated with a particular frequency bandwidth [104].

The determination of each IMF bandwidth follows a methodical procedure [105,106]. Initially, the Hilbert transform is utilized to derive the spectrum of every $u_{(k)}$. This spectrum is subsequently transferred to the baseband section by aligning it with an estimated center frequency. The final step involves estimating the bandwidth by evaluating the Gaussian smoothness of the demodulated signal, which is derived from the parametric gradient squared. The primary goal of the VMD methodology is to decrease the calculated bandwidths of the modes while guaranteeing that their aggregate accurately reconstructs the original signal. This process is framed as a constrained variational problem [103], formalized in Equation 18:

$$min_{\{u_k\},\{\omega_k\}}\{\sum\nolimits_k \|\delta_t\left[\left(\delta(t)+\frac{j}{\pi t}\right)^{*}u_k(t)\right]e^{-jw_k t}\|_2^2 subject to \sum\nolimits_k u_k(t) = f(t) \tag{18}$$

With t representing the time. $\boldsymbol{\omega}_k$: denotes the central frequency of the k^{th} mode. f(t) is the input signal, and δ (t) refers to the unit pulse function

To effectively integrate the constraint into the optimization framework, an enhanced Lagrange multiplier λ is employed, which allows for a unified representation of the constraint within the objective function L [17].

$$L_{(\{u_k\},\{\omega_k\},\lambda)} = \alpha\sum_k \|\delta_t\left[\left(\delta(t)+\frac{j}{\pi t}\right)^{*}u_k(t)\right]e^{-jw_k t}\|_2^2 + \|f(t) - \sum_k u_k(t)\|_2^2 + \left\langle \lambda(t), f(t) - \sum_k u_k(t)\right\rangle \tag{19}$$

With α denoting a quadratic penalty parameter used to ensure the accuracy of the signal reconstruction [17,107].

The proposed prediction framework

The present research introduces a structured evaluation framework for photovoltaic (PV) power forecasting models, incorporating both machine learning (ML) and deep learning (DL) techniques, including LSTM, BiLSTM, GRU, BiGRU, CNN, Inception, Residual Networks, ANN, SVM, and Random Forest. These models are assessed using real-world data from a 53 MW grid-connected PV plant in Djelfa, Algeria, spanning the period from January 2018 to December 2019. Forecasting performance is evaluated across two temporal horizons—30 min and 3 h—while monthly analyses provide detailed insights into the variability of each model's performance under different climatological conditions. As an advanced methodological enhancement, Variational Mode Decomposition (VMD) is applied to decompose complex PV power signals into distinct and interpretable modes, thereby enriching the quality of inputs fed into the forecasting models. The proposed framework aims to support data-driven decision-making and enable the seamless integration of large-scale PV power into the energy mix. The study's contribution is articulated through several key components, each targeting a critical aspect of accurate and resilient PV forecasting. The detailed steps of the proposed methodology are illustrated in Fig. 6 and outlined as follows:

1 **Data Collection and Preprocessing:** The initial phase of the study is focused on detailed data collection and comprehensive processing. Essential activities in this stage encompass rectifying missing values, identifying and removing anomalies, and excluding non-essential nighttime data. Then, data is strategically partitioned into separate subsets for training and testing purposes, 80 % and 20 %, respectively.

2 **Training and optimizing the predictive models:** In this stage, the ML and DL modes undergo a rigorous tuning process through a grid search methodology that is appropriate for each model. This process aimed at identifying the most effective hyper-parameters, ensuring the model's ability to deliver precise and reliable PV power forecasts.

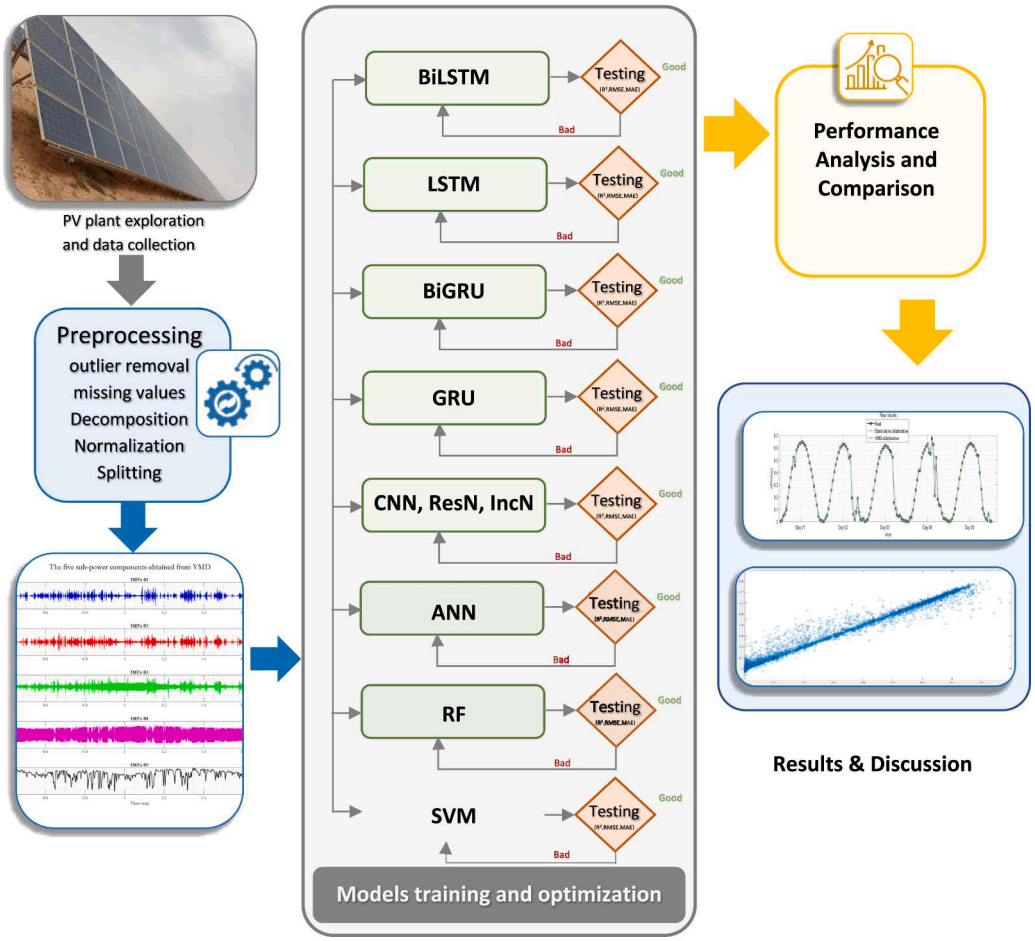

Fig. 6. Flow chart of the Methodology.

3 **Initial Stand-alone Performance Comparison:** After being trained and optimized on the same input data, models undertake a comparative analysis to assess their baseline forecasting capabilities. The evaluation is performed using a range of metrics such as the Mean Absolute Error (*MAE*), Mean Square Error (*MSE*), normalized Root Mean Square Error and (nRMSE), and the determination coefficient (R^2), whose mathematical expressions are listed below. This analysis is critical in understanding each model's advantages and disadvantages in real-world scenarios.

$$\boldsymbol{R}^2(\%) = 1 - \frac{\sum_{i=1}^{n}\left(\boldsymbol{I}_{i,measured} - \boldsymbol{I}_{i,predicted}\right)^2}{\sum_{i=1}^{n}\left(\boldsymbol{I}_{i,measured} - \widehat{\boldsymbol{I}}_{i,measured}\right)^2} \tag{20}$$

$$\boldsymbol{RMSE} = \sqrt{\frac{\sum_{i=1}^{n}\left(\boldsymbol{I}_{i,predicted} - \boldsymbol{I}_{i,measured}\right)^2}{\boldsymbol{N}}} \tag{21}$$

$$\boldsymbol{nRMSE}(\%) = \frac{\boldsymbol{RMSE}}{\boldsymbol{Max}(\boldsymbol{I}_{measured}) - \boldsymbol{Min}(\boldsymbol{I}_{measured})} * 100 \tag{22}$$

$$\boldsymbol{MAE} = \frac{1}{\boldsymbol{n}}\sum_{i=1}^{n}\left|\boldsymbol{I}_{predicted,i} - \boldsymbol{I}_{measured,i}\right| \tag{23}$$

$$\boldsymbol{nMAE}(\%) = \frac{\boldsymbol{MAE}}{\boldsymbol{Max}(\boldsymbol{I}_{measured}) - \boldsymbol{Min}(\boldsymbol{I}_{measured})} * 100 \tag{24}$$

R2 measures the extent to which the predicted values match the actual target values by assessing their alignment with the ideal 1:1 line. An elevated R2 indicates a stronger model, as the simulated values are nearer to the real ones. RMSE is useful for detecting large errors due to its sensitivity to outliers; the squaring of errors amplifies the impact of extreme values. However, RMSE can be misleading if the data contains outliers, as these can disproportionately influence the metric. MAE provides a straightforward indicator of the mean forecasting error by taking the absolute differences between predicted and actual values. Unlike R2 and RMSE, MAE doesn't allow positive and negative errors to cancel each other out, offering a clear view of the typical error magnitude [108–112].

4 **Variational Mode Decomposition:** After the initial comparison, VMD is employed to decompose and extract features from the non-stationary characteristics of the PV generation signal. This technique decomposes the signal into a series of IMFs, each representing distinct frequency components within a limited bandwidth.

5 **Second VMD Performance-based Comparison:** VMD generates IMFs signals that are fed into all ML and DL models. A comparison is performed here the investigate the influence of VMD on the performance of each model. Interesting insights are then derived.

6. Seasonal and Monthly Analysis: The next step is to delve deeper into understanding the model's patterns within the data, particularly during specific times of the year, and to analyze their seasonal variations. This involves not only recognizing recurring trends but also identifying the underlying factors driving these fluctuations across different months. Such an approach offers a clearer and more practical representation of the model's temporal dynamics and response patterns.

Results and discussion

Data collection, preprocessing, and splitting

This research utilizes a dataset comprising 21,046 measurements of PV generation, recorded from 2018 to 2019 at the Djelfa PV plant. The data recording spans from 6 a.m. to 8p.m., with recordings taken every 30 min. Recognizing the importance of power supply systems in intraday forecasting, the temporal resolution was altered from 30-minute to 3-hour intervals, as demonstrated in Fig. 7. This adjustment is considered a more practical approach for evaluating the Djelfa PV plant's intraday capacity and optimizing grid coordination. To provide a comprehensive analysis, the study examines both 30-minute and 3-hour forecasting intervals. For all simulations, the dataset is partitioned into two complementary subsets: the training set, accounting for 80 %, and the testing set comprising the remaining 20 % of the whole dataset.

The constructed model may inherently exhibit biases due to anomalies or outliers that are present within the dataset, and sometimes due to variations in the scale of input data, which arise from differing maximum ranges across their different nature. To tackle these issues, the process of data normalization is essential to mitigate the influence of outliers and ensure that all features are standardized to a uniform scale. In this study, the Min-Max standardization method is applied, as detailed in equation (7) [113]:

$$\overline{X}_i = \frac{X_i - X_{min}}{X_{min} - X_{max}} \tag{7}$$

Where $\overline{X}_i$ represents the normalized data, X_i Denotes the original data. X_{min} , X_{max} Refers to minimal and maximal values contained in the dataset.

Another important consideration in the preprocessing step is related to the requirements of the CNN. Although the model performs 1D convolutions, the input data must be reshaped into a 3D format to meet the input requirements of the CNN. In this context, the three dimensions correspond to the number of samples, the number of features (which represent historical time steps or delay points), and the number of channels (typically set to 1 for 1D CNNs, indicating a single data channel). This reshaping is essential because CNNs, regardless of performing 1D convolutions, are designed to process data in a 3D structure, allowing them to efficiently learn spatial or temporal patterns within the sequences. The transformation ensures that each input sequence is processed correctly and aligned with the model's expectations, enabling it to effectively learn from the data during both the training and testing phases of the forecasting task.

Hardware and software requirements

The development of the model is carried out in the MATLAB R2018b environment, and all modeling scenarios were executed on a portable computer with hardware specifications including a 64-bit OS, 16.00 GB RAM, and an Intel(R) Core processor (TM) i7-9850H CPU @ 2.60 GHz.

The model's parameters

The accuracy of predictive models is affected by several factors, such as the volume of training data, hyperparameters, network architecture, and optimizer algorithms used for weight and bias optimization [45]. Recognizing the impact of these factors, an initial step of hyperparameter tuning was undertaken by exploring various combinations of hyperparameters to identify the most effective setup for each model, ensuring they are well-calibrated and capable of delivering high accuracy. This involves adjusting factors such as learning rates, batch sizes,

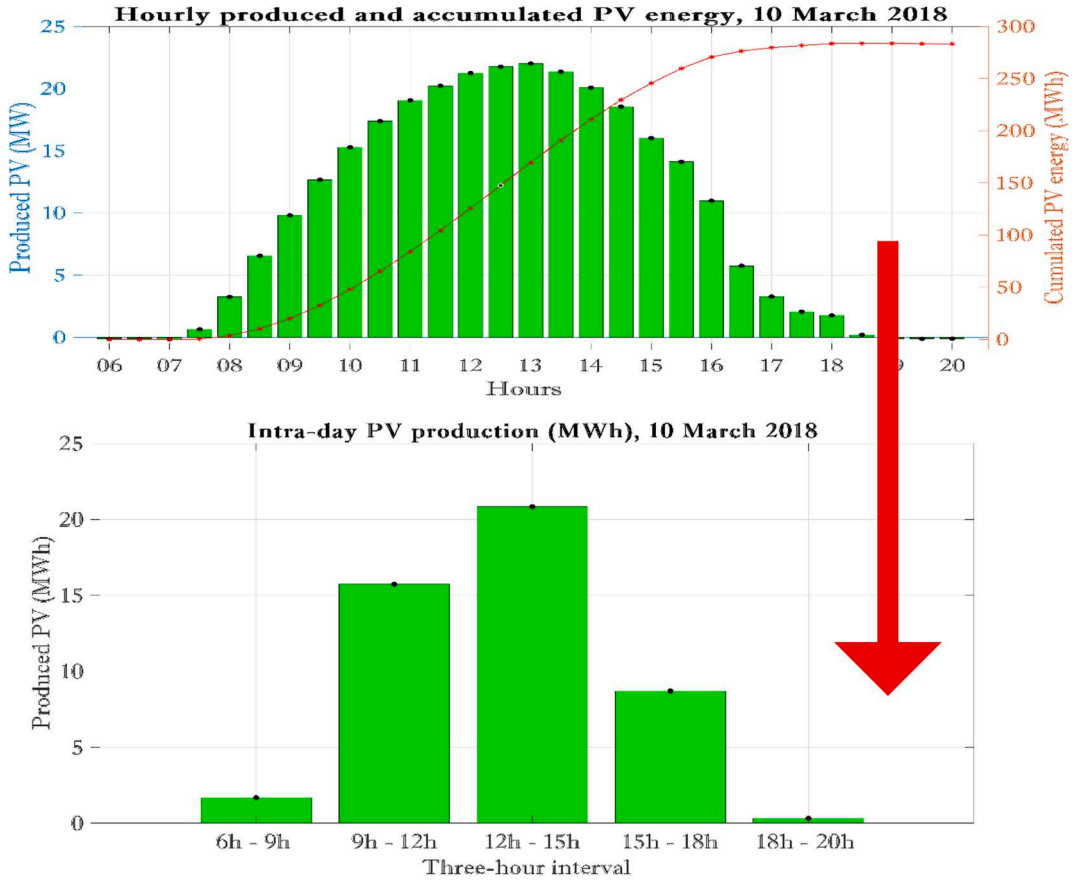

Fig. 7. The temporal resolution conversion.

layer numbers, and units within the network, among others. Once the optimal hyperparameters were identified, they were employed during the aggregation phase, where models were compared and combined to build the global model. This step is crucial for harnessing the advantages of each model and achieving a robust and reliable global predictive algorithm. Table 3 elucidates the hyperparameters tested for each algorithm during the grid search procedure.

Results and discussion

Stand-alone results

In all simulations conducted, a fixed time delay of four is applied. This implies that each prediction is generated by utilizing the latest four historical input data points, thereby guaranteeing that each model is based on a consistent and recent historical context, which is crucial for accurate forecasting. For each algorithm, two models are built: one for the short-term horizon (30 min) and another for the medium-term horizon (3 h). This approach allows for assessing the impact of training data volume on model effectiveness and evaluating the models' robustness across different time scales. The performance of each model, assessed based on the selected statistical indicators, is systematically presented in Table 4. All indicators are computed using normalized data to enable equitable comparisons across datasets from diverse power plants, regions, or capacity scales (e.g., kW, MW, GW). This standardized approach ensures a rigorous performance analysis, offering valuable insights to the scientific community and interested researchers.

For the 30-minute ahead forecasting horizon, the results show that the CNN model provides the most accurate predictions and the least error among the models tested, with an R^2 of 0.9678, the lowest RMSE (0.0471), and the lowest nRMSE (0.0545). These findings demonstrate the superior ability of CNN to automatically extract and learn complex spatial patterns from the input data through its convolutional layers, which effectively capture localized features and correlations within the PV power signals, that are crucial for modeling intricate temporal dynamics [114,115]. The BiLSTM model, with an R^2 of 0.9631, also demonstrates strong performance, leveraging its bidirectional architecture to analyze input sequences in both forward and backward directions. This enables BiLSTM to capture contextual dependencies and intricate temporal patterns within the PV power signals, enhancing its ability to predict future values with high accuracy [116]. Similarly, the inception module performs well, achieving an R^2 of 0.9523. Its strength lies in its ability to process multi-scale features simultaneously by combining different filter sizes within its architecture [59,95]. This allows the inception module to capture a wide range of patterns, from localized fluctuations to broader trends, making it particularly effective for complex and diverse forecasting tasks [117]. The residual module, with an R^2 of 0.9182, exhibits its effectiveness by utilizing skip connections to address the vanishing gradient problem and maintain the integrity of feature propagation. This architecture enhances its ability to model long-term dependencies and subtle variations in PV power signals, contributing to its competitive performance [118,119]. In contrast, traditional machine learning algorithms such as ANN, SVM, and RF show comparatively lower performance, with R^2 values of 0.8656, 0.8726, and 0.8302, respectively. Among these, SVR has the lowest R^2 (0.8302), indicating its limited capacity to generalize and adapt to the complexities of PV power forecasting.

In the 3-hour ahead forecasting scenario, CNN continues to outperform all other models, with an R^2 of 0.9839 and the lowest RMSE (0.0371). Other deep learning models, particularly BiLSTM, Inception, and residual modules, also show strong results compared to ML. Interestingly, machine learning models (ANN, RF, SVR) improve their performance in this longer horizon, particularly RF, which achieves an R^2 of 0.9138. The enhanced performance of RF, in particular, may be attributed to its ensemble-based architecture, which combines multiple decision trees to effectively generalize and capture important features over a larger prediction window. The ANN model benefits from its flexible architecture, which allows it to capture generalized patterns and adapt to longer prediction sequences where the temporal dynamics may be less intricate. This adaptability likely contributes to its enhanced performance over longer horizons. Similarly, SVR demonstrates better accuracy potentially due to its reliance on kernel-based methods, which enable it to model broader trends effectively when the need for detailed temporal resolution is reduced. This improvement suggests that ML models may be more effective when less historical data is available. These findings highlight the importance of evaluating multiple models to uncover varying data dynamics, providing deeper insights into the unique strengths of each algorithm and supporting more informed decision-making, ultimately leading to improved prediction accuracy.

Variational model decomposition results

As discussed in the previous sections, VMD is utilized to decompose the time series signal into IMFs. In this study, the PV power signal is decomposed into five distinct IMFs, as illustrated in Fig. 8. These IMFs are then used as inputs to the various models for forecasting. The performance results of these models, based on the decomposed IMFs, are comprehensively detailed in Table 5.

Applying VMD for the 30-minute ahead forecasting horizon, the hybrid models exhibit significant performance improvements compared to the standalone models discussed previously (see Table 5). In this case, models are better equipped to isolate relevant information and analyze the intrinsic components of the data, enabling them to capture complex patterns and dynamics that may otherwise remain undetected in the raw data. This enhanced processing of the data contributes to more accurate predictions, underscoring the effectiveness of VMD as a preprocessing

Table 4
Stand-alone results.

Horizon	30 min					3 hours				
Metrics	MAE	nMAE (%)	RMSE (MW)	nRMSE (%)	R^2	MAE	nMAE (%)	RMSE (MW)	nRMSE (%)	R^2
LSTM	0.0621	7.180	0.0934	10.82	0.8734	0.0760	8.520	0.1058	11.85	0.8687
BiLSTM	0.0278	3.220	0.0504	5.840	0.9631	0.0362	4.050	0.0520	05.83	0.9682
GRU	0.0567	6.560	0.0917	10.61	0.8780	0.0710	7.950	0.1000	11.21	0.8826
BiGRU	0.0498	5.760	0.0878	10.16	0.8882	0.0568	6.360	0.0869	9.730	0.9114
CNN	**0.0251**	**2.900**	**0.0471**	**5.450**	**0.9678**	**0.0281**	**3.150**	**0.0371**	**4.150**	**0.9839**
Resnet	0.0423	4.900	0.0751	8.690	0.9182	0.0469	5.250	0.0645	7.220	0.9512
Incepnet	0.0364	4.220	0.0573	6.640	0.9523	0.0431	4.820	0.0726	8.140	0.9381
ANN	0.0529	6.120	0.0963	11.14	0.8656	0.0599	6.710	0.0882	9.880	0.9088
RF	0.0507	5.870	0.0937	10.85	0.8726	0.0960	5.640	0.0857	9.600	0.9138
SVR	0.0818	9.470	0.1082	12.52	0.8302	0.0564	6.320	0.1063	11.91	0.8675

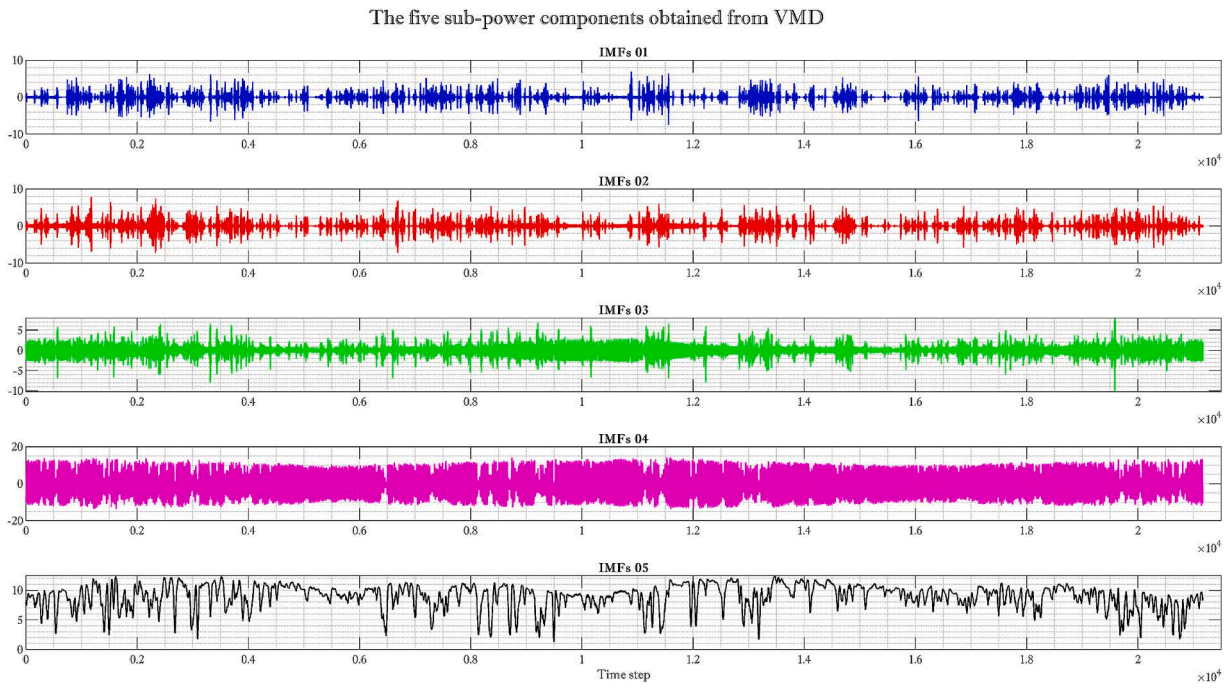

Fig. 8. The segments produced through VMD.

Table 5
VMD based results.

Horizon	30 min					3 hours				
Metrics	MAE	nMAE (%)	RMSE	nRMSE (%)	R^2	MAE	nMAE (%)	RMSE	nRMSE (%)	R^2
LSTM	0.0281	3.250	0.0434	5.020	0.9727	0.0272	3.040	0.0367	4.110	0.9842
BiLSTM	0.0243	2.820	0.0373	4.320	0.9798	0.0286	3.210	0.0389	4.350	0.9822
GRU	0.0153	1.770	0.0251	2.900	0.9909	0.0161	1.800	0.0218	2.440	0.9944
BiGRU	0.0142	1.650	0.0225	2.600	0.9927	0.0171	1.910	0.0228	2.550	0.9939
CNN	0.0205	2.370	0.0318	3.680	0.9854	0.0289	3.240	0.0389	4.360	0.9822
Resnet	0.0291	3.370	0.0414	4.790	0.9752	0.0356	3.990	0.0518	5.800	0.9686
Incepnet	0.0350	4.050	0.0522	6.050	0.9604	0.0524	5.700	0.0759	8.500	0.9324
ANN	0.0093	1.08	0.0163	1.890	0.9961	**0.0090**	**1.100**	**0.0125**	**1.400**	**0.9982**
RF	0.0377	4.37	0.0610	7.060	0.9459	0.0350	3.920	0.0525	5.880	0.9676
SVR	0.0333	3.86	0.0415	4.800	0.9750	0.0339	3.800	0.0461	5.160	0.9751

technique for improving forecasting performance.

Although deep learning algorithms outperformed machine learning models in the initial experiment, the ANN, a ML model, excelled when paired with VMD preprocessing, securing the top position with an R^2 value of 0.9961, followed by VMD-BiGRU and VMD-GRU, with R^2 values of 0.9927 and 0.9909, respectively. The error metrics; RMSE, nRMSE, MAE, and nMAE, also showed substantial reductions with VMD-based models. This improvement is particularly pronounced in machine learning techniques, while deep learning models showed only slight enhancements. These findings suggest that ML models benefit more from effective feature engineering, which enhances their performance. In the case of the ANN, decomposing the original PV signal into a finite set of IMFs, each representing distinct oscillatory modes at different frequency bands enables the model to focus on the most informative data by providing clearer, noise-reduced inputs, which enhances its ability to generalize. While deep learning models like BiGRU and GRU are effective at capturing temporal dependencies, the VMD-preprocessed ANN benefits from a simpler architecture that can learn and predict more efficiently, achieving superior performance with less complexity and computational demand. In summary, the application of VMD preprocessing allows ML models to achieve more accurate predictions with fewer data and less complexity, while DL models, which rely more on automatic feature extraction, show only marginal improvements. Therefore, careful data preprocessing and thoughtful model selection are essential for accurate feature understanding, extraction, and tuning, as well as for precise PV power forecasting. The scatter plot of these results is illustrated in Fig. 9.

The performance of the models significantly improves when using the 3-hour ahead forecasting horizon, which is based on a smaller dataset of 725 samples, compared to the 30-minute horizon, which utilizes a larger dataset of 5,288 samples. The impact of smaller datasets on model performance is noteworthy. While larger datasets are typically expected to improve model accuracy, in this case, the smaller dataset leads to better performance. Larger datasets can introduce noise, irrelevant features, or overfitting, which can complicate the learning process and increase error rates. In contrast, the smaller dataset, when preprocessed with VMD, provides cleaner and more relevant data, allowing the models to focus on the most important features and generalize

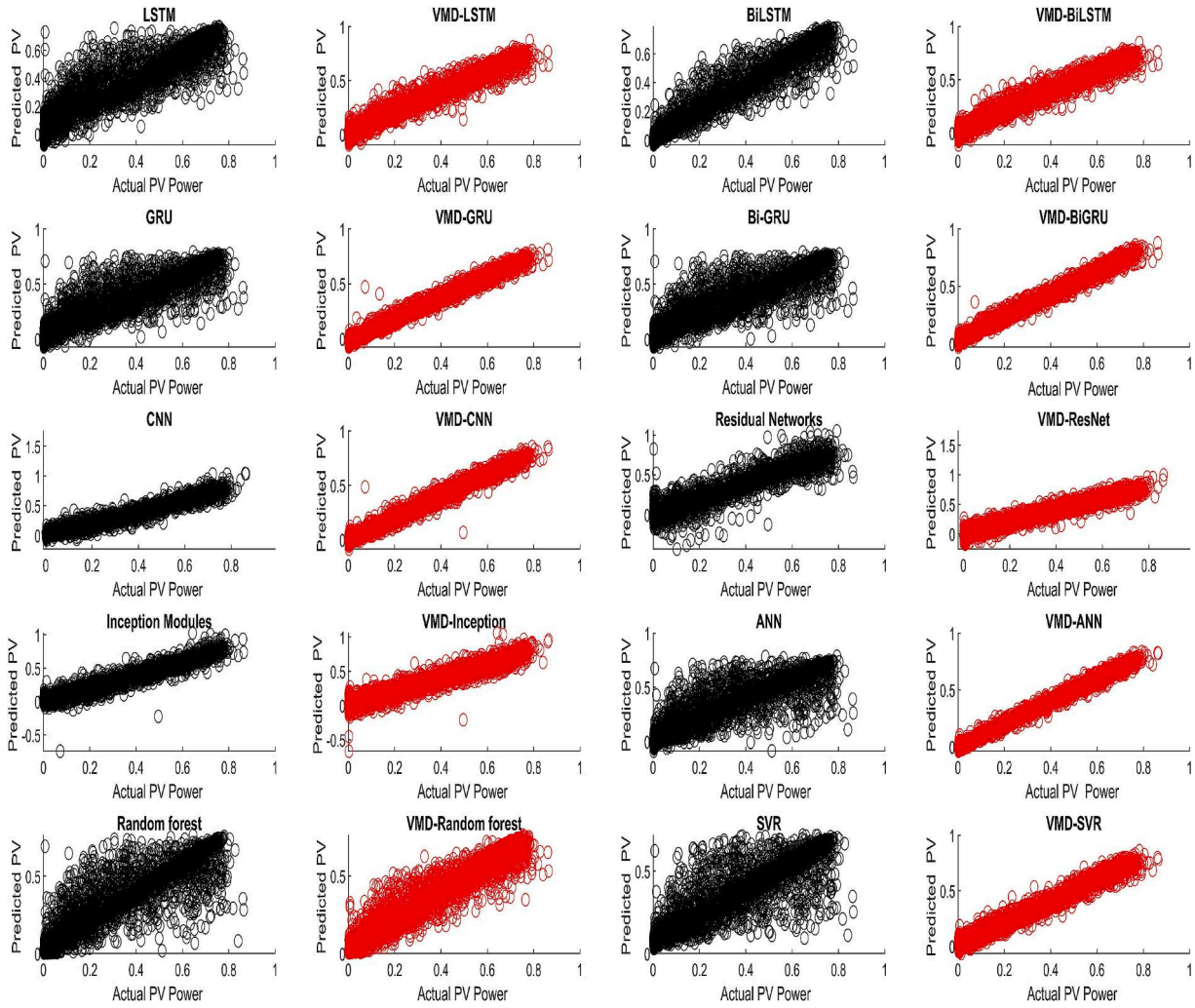

Fig. 9. Scatter plot for 30 min ahead.

better. Thus, the smaller dataset, combined with VMD, reduces model complexity and computational demands, while simultaneously enhancing prediction accuracy. This further confirms the value of VMD preprocessing in improving forecasting performance. The scatter for the 3-hour ahead horizon, as shown in Fig. 10, reinforce the effectiveness of VMD-based preprocessing, with even better performance than observed in the 30-minute horizon. The R^2 values are exceptionally high for the 3-hour ahead forecasts, with the VMD-ANN model nearly perfect at 0.9982. The DL models, particularly GRU, BiGRU, LSTM, BiLSTM, and CNN, maintain strong R^2 values (0.9944, 0.9939, and 0.9942, 0.9822, and 0.9822 respectively), demonstrating their robustness across longer forecasting horizons when combined with VMD. RMSE and nRMSE continue to decrease, reflecting improved accuracy. The VMD-ANN model once again performs exceptionally well, with RMSE dropping to 0.0125 and nRMSE to 0.0140. The consistency in low error metrics across all models indicates that VMD preprocessing enhances model performance by effectively decomposing the input data into modes that are easier for these models to learn from. The results suggest that incorporating VMD as a preprocessing step significantly improves the performance of both DL and ML models.

Fig. 11 presents the boxplots of the absolute errors for both standalone and VMD-based models, corresponding to 30-minute and 3-hour ahead forecasting, respectively. As seen in these figures, VMD decomposition significantly reduces error values, with a clear shift toward smaller errors. This reduction is especially noticeable in the 3-hour horizon, where the smaller dataset, coupled with VMD preprocessing, leads to more accurate predictions. The boxplots reveal narrower interquartile ranges and lower median values for VMD-based models, indicating greater consistency and reliability compared to standalone models. The reduction in error values demonstrates that VMD enhances model performance by decomposing input data into more manageable components. This process allows the models to focus on the most relevant patterns, improving both accuracy and generalization. The substantial improvement in forecasting accuracy across both horizons further emphasizes the effectiveness of VMD preprocessing in optimizing model performance.

Given the widespread adoption of photovoltaic (PV) power forecasting, it is both appropriate and necessary to evaluate the performance of the proposed model in relation to existing studies. Nevertheless, it is crucial to recognize the inherent challenges in such comparisons, primarily due to significant variations in key aspects such as the types of forecasting algorithms employed, the nature of the datasets used (typically originating from distinct climatological regions) and the differing temporal forecasting horizons. These factors collectively influence model behavior and performance, often leading to disparities across case studies and rendering direct comparisons potentially inequitable. Despite these limitations, we have carefully selected and cited studies in Table 6 that, in our judgment, share sufficient methodological or contextual commonalities with our work to serve as a meaningful basis for comparative analysis.

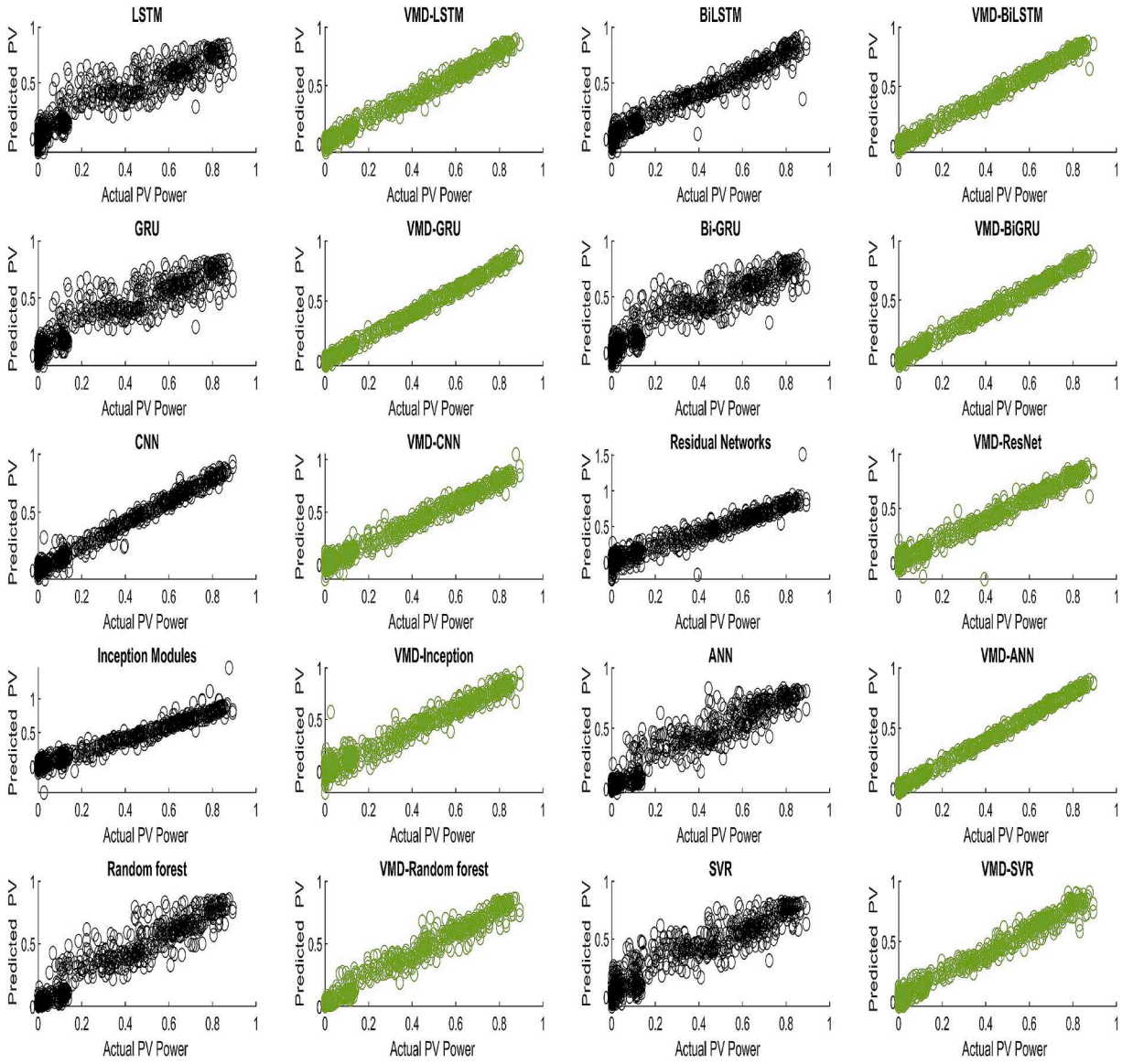

Fig. 10. Scatter plot for 3 h ahead forecasting.

Monthly assessment results

The monthly variation in forecasting performances, as depicted in Figs. 12–17 highlights the performance of VMD-based models in PV power forecasting for both short-term (30 min) and medium-term (3 h) forecasting horizons. The VMD-based model exhibits remarkable robustness across different months, maintaining high accuracy and low error metrics regardless of seasonal variations. This suggests that VMD effectively handles the inherent variability in PV power generation data throughout the year. Analyzing the results in terms of the best and worst-predicted months reveals interesting insights into the performance of the forecasting models. June stands out as the best-predicted month across both the 3-hour and 30-minute forecasting horizons, particularly for the VMD-based models. During the 3-hour ahead forecast, the VMD-based model achieves an R^2 varying from 0.9990 to 0.9834, for all tested models, which is one of the highest across all months, indicating near-perfect predictive ability. The RMSE is ranging from 0.0084 to 0.0342, and the MAE is minimized to (0.0057–0.0253). When a 30-minute ahead forecast is applied, the VMD-based model also shows excellent performance, with an R^2 ranging from 0.9850 to 0.9990, which is the highest among all months. The RMSE and MAE values range also from 0.0298 to 0.0077 and from 0.0239 to 0.044, respectively, which are the lowest, confirming June as the best-predicted month. This superiority could be attributed to more stable weather patterns and consistent solar radiation, making it easier for the models to predict PV power generation accurately.

On the other hand, November appears to be the worst-predicted month. For the 3-hour ahead forecast, November records the lowest R^2 value ranging from 0.7716 to 0.997, for all models, indicating the least accurate predictions. The RMSE and MAE values are also relatively high and vary from 0.042 to 0.1351 and from 0.0312 to 0.100, respectively, reflecting greater prediction errors. For the 30-minute ahead forecast, the stand-alone models show the lowest R^2 varying from 0.7483 to 0.9622, along with higher RMSE (0.0520—0.1341) and MAE (0.0303–0.1018) compared to other months, making it the least accurate month in short-term forecasts as well. Even with VMD preprocessing, while performance improves significantly, November still ranks lower compared to other months, with higher RMSE and MAE values (Figs. 13 and 14). This could be due to the increased variability in solar conditions during November, possibly because of more frequent cloud cover, lower solar angles, and shorter daylight hours, which introduce additional challenges for accurate forecasting.

To offer a clearer view of daily forecasting performance under

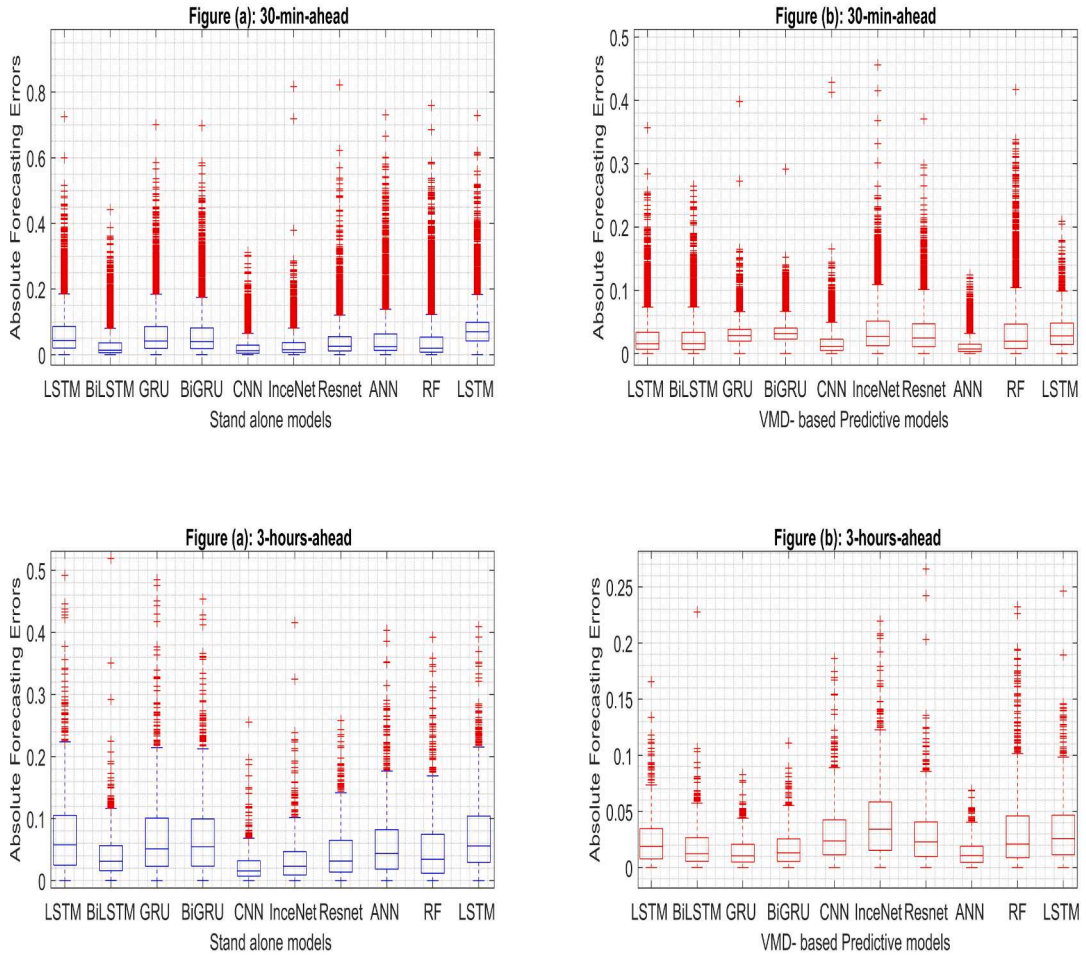

(a): Standalone model (30 min ahead), (b) VMD-based models (30 min ahead)

(c): the standalone model (3h), (d) VMD-based models (3h ahead)

Fig. 11. Boxplot of the absolute errors for: (a): Standalone model (30 min ahead), (b) VMD-based models (30 min ahead) (c): the standalone model (3 h), (d) VMD-based models (3 h ahead).

Table 6
Comparison of Model Performance with Previous Studies.

Region	Method	Horizon	Metrics
Iran [120]	GBR	Not mentioned	$R^2 = 98$ %
China [59]	IEDN-RNET	Short/ medium	nMAE = 16.9 %, nRMSE = 4.51 %, $R^2 = 0.98052$
USA [60]	TCM- LSTM-RNN	1 day	RMSE = 6.29 %, MAE = 2.78 % r = 96.19 %
Turkey, Malaysia [61]	MWSO-RBFN	15 min	NSE = 0.979
Australia, Algeria [47]	NARX	5, 15, 30, 60 min	10 % < rRMSE < 20 % $0.919 < R^2 < 0.971$
Algeria [63]	ANN	Not mentioned	MAE = 1.998, $R^2 = 0.997$,
Algeria [121]	TVF-EMD-ELM	30 min	nMAE = 1.58, nRMSE = 2.27, r = 99.94
This work (Algeria)	CNN	30 min	nMAE = 2.9 %, nRMSE = 5.45 %, $R^2 = 0.9678$
		3 h	nMAE = 3.15 %, nRMSE = 4.15 %, $R^2 = 0.9839$
	VMD-ANN	30 min	nMAE = 1.08 %, nRMSE = 1.89 %, $R^2 = 0.9961$
		3 h	nMAE = 1.1 %, nRMSE = 1.4 %, $R^2 = 0.9982$

various weather conditions for the 30-minute-ahead horizon, Fig. 18 presents four representative days with distinct weather patterns. The CNN model, identified as the best-performing standalone approach, effectively follows the general trends of the actual data. On the other hand, VMD-ANN, the top-performing model among the hybrid approaches, not only preserves this trend-following ability but also achieves higher precision and accuracy, particularly during periods of rapid variation. This demonstrates the benefit of integrating VMD as a preprocessing step to enhance the model's responsiveness to dynamic weather conditions.

Conclusion and recommendations

This research thoroughly evaluates the performance of various machine learning, and deep learning models, including LSTM, BiLSTM, GRU, CNN, Inception, Residual modules, ANN, SVM, and Random Forest, for photovoltaic power forecasting. Models were developed for both 30-minute and 3-hour forecasting horizons, with a comprehensive assessment based on monthly performance metrics such as RMSE and MAE. A crucial aspect of the study was the incorporation of Variational Mode Decomposition for feature extraction, followed by seasonal analysis to explore recurring trends and model interactions. The findings challenge the prevailing assumption that deep learning always outperforms machine learning in PV forecasting. Results indicate that ML

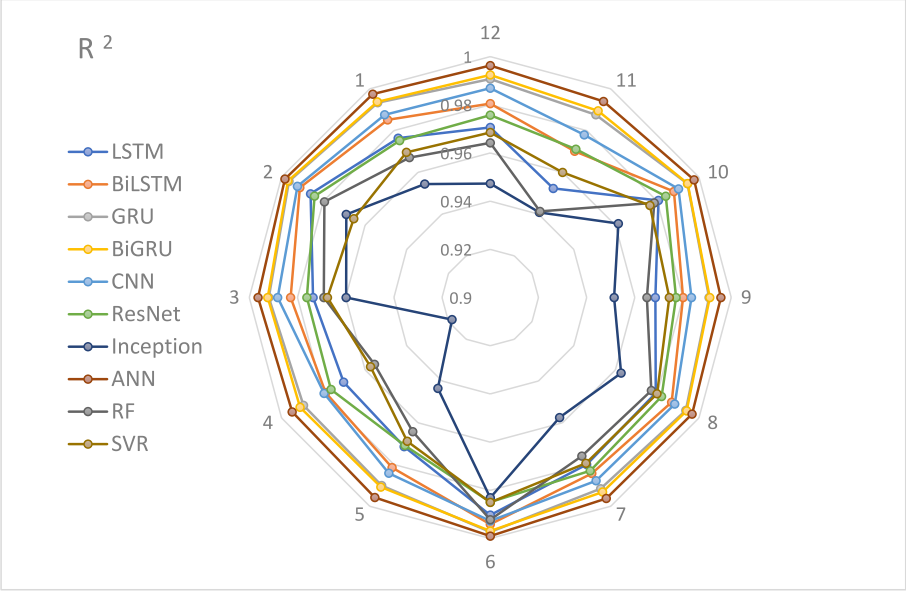

Fig. 12. Monthly variation of R-squared the developed models (30 min ahead).

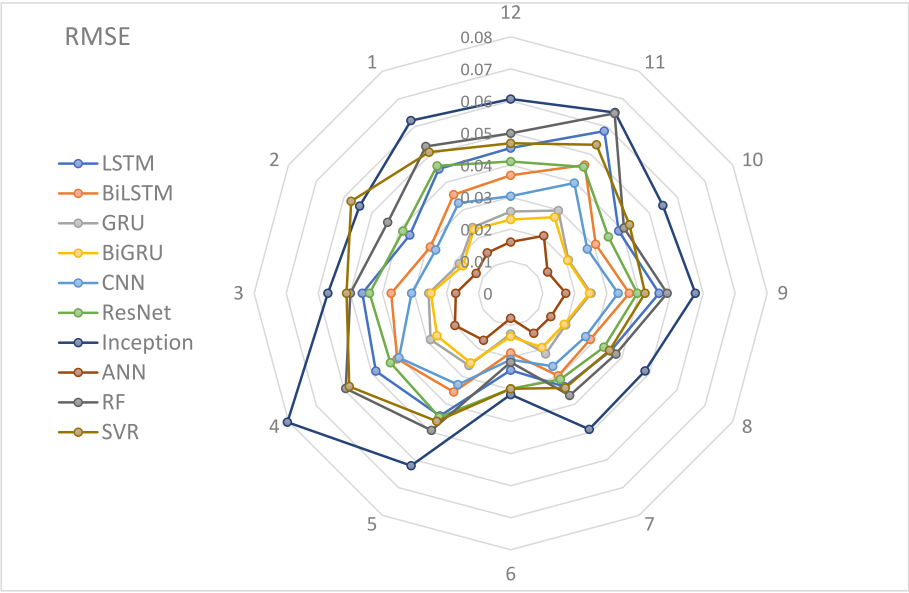

Fig. 13. Monthly variation of RMSE for the developed models (30 min ahead).

models, particularly ANN, RF, and SVM, benefit more from VMD preprocessing than DL models, often achieving superior accuracy across various conditions. This suggests that the synergy between ML models and advanced signal decomposition techniques can be more effective than complex DL architectures alone, especially for certain forecasting horizons and seasonal variations. These insights highlight the importance of selecting the right combination of models and preprocessing techniques to maximize forecasting accuracy, leading to better grid integration, improved decision-making, and enhanced energy management. These advancements are essential for the broader renewable energy sector, particularly photovoltaic energy, playing a key role in advancing the global energy transition and supporting sustainable energy systems worldwide. The results yield several key conclusions related to the Djelfa case study that should be taken into account by practitioners and decision-makers, including the following:

- In case of standalone model, it is important to prioritize the use of deep learning models, particularly CNN, as they consistently outperform all standalone models for both the 30-minute and 3-hour forecasting horizons, demonstrating their capacity to efficiently capture complex data patterns and dynamics for this region.
- Adopt Inception and Residual modules in model design to improve forecasting performance. The strength of inception modules lies in its ability to process multi-scale features simultaneously by combining different filter sizes within its architecture, enabling the capture of wide range of patterns, from localized fluctuations to broader trends, making it particularly effective for complex and diverse forecasting tasks. The residual module exhibits its effectiveness by utilizing skip connections to address the vanishing gradient problem and maintain the integrity of feature propagation
- Utilize machine learning models such as ANN, Random Forest, and SVR for longer forecasting horizons, especially when historical data

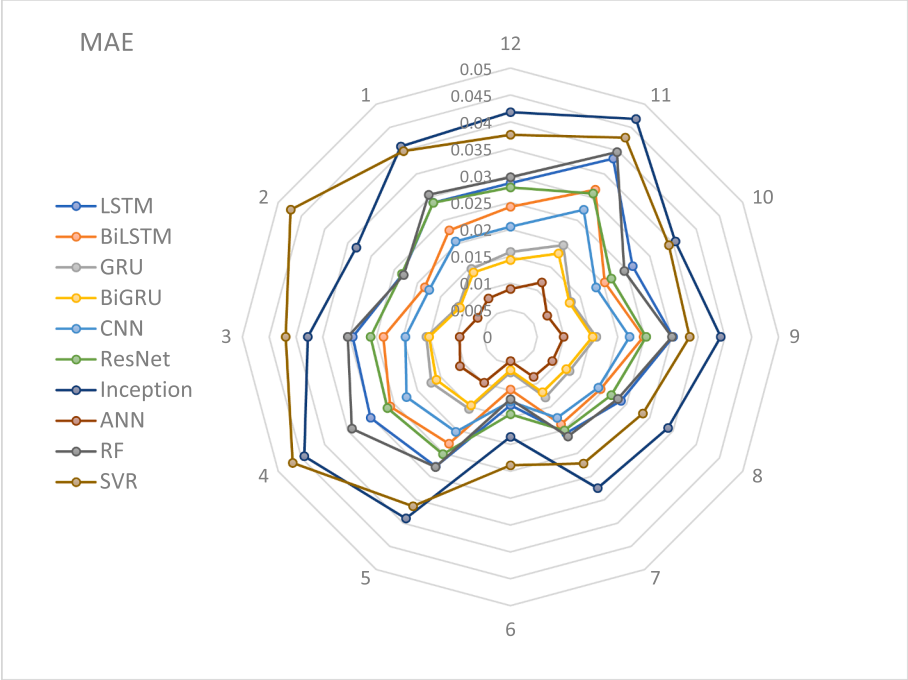

Fig. 14. Monthly variation of MAE for the developed models (30 min ahead).

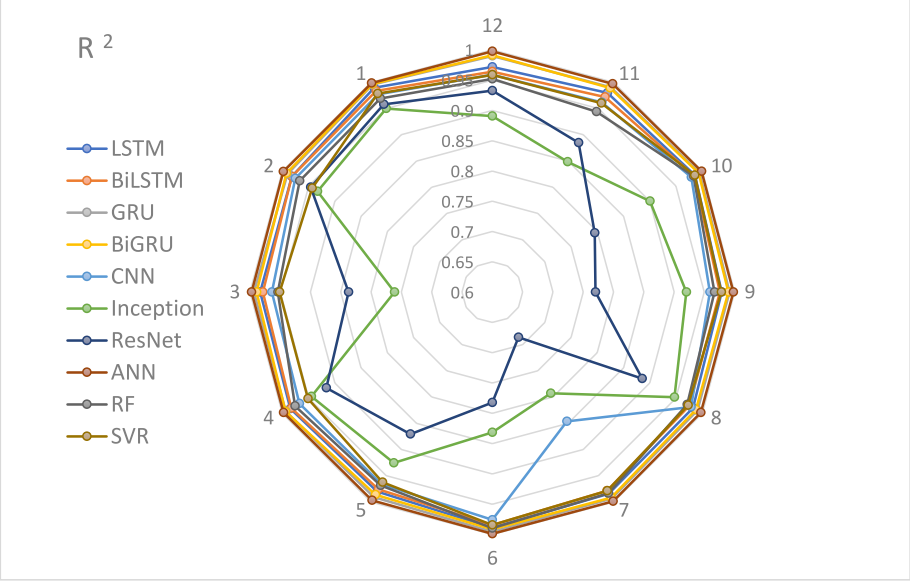

Fig. 15. Monthly variation of R-squared the developed models (3 h ahead).

is limited. These models have shown higher effectiveness in such contexts, whereas deep learning models should be leveraged when larger datasets are available due to their superior ability to model complex data relationships.

- Incorporate Variational Mode Decomposition (VMD) as a preprocessing step to enhance model accuracy. VMD preprocessing significantly enhances model performance, especially for machine learning models, which benefit more from effective feature engineering. While deep learning models leverage automatic feature extraction, VMD aids both ML and DL models by decomposing input data into cleaner, more relevant components, improving generalization and accuracy.
- Take seasonal variability into account during model training and evaluation, as VMD-based models demonstrate variable accuracy across different months. For instance, June shows the highest prediction accuracy while November performs the worst. This seasonal variability highlights the influence of environmental and temporal factors on forecasting accuracy, further emphasizing the importance of meticulous data preprocessing and model tuning.
- To further advance the effectiveness and applicability of the proposed forecasting framework, the following extensions can be considered:
- **Investigating alternative decomposition and signal processing techniques** such as Empirical Mode Decomposition (EMD) and Wavelet Transform (WT), is recommended to extract more detailed signal characteristics. These approaches have the potential to enhance forecasting performance by capturing intricate temporal patterns in the data.

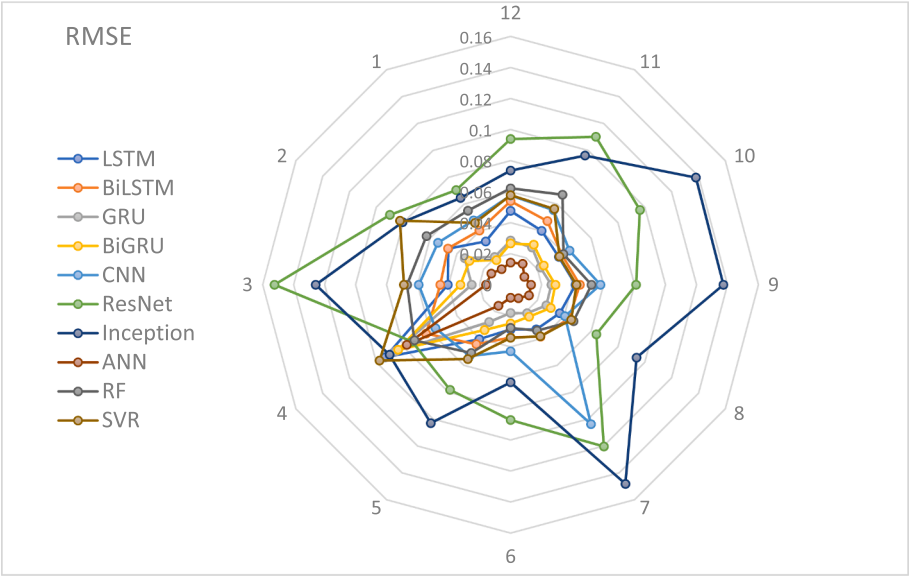

Fig. 16. Monthly variation of RMSE the developed models (3 h ahead).

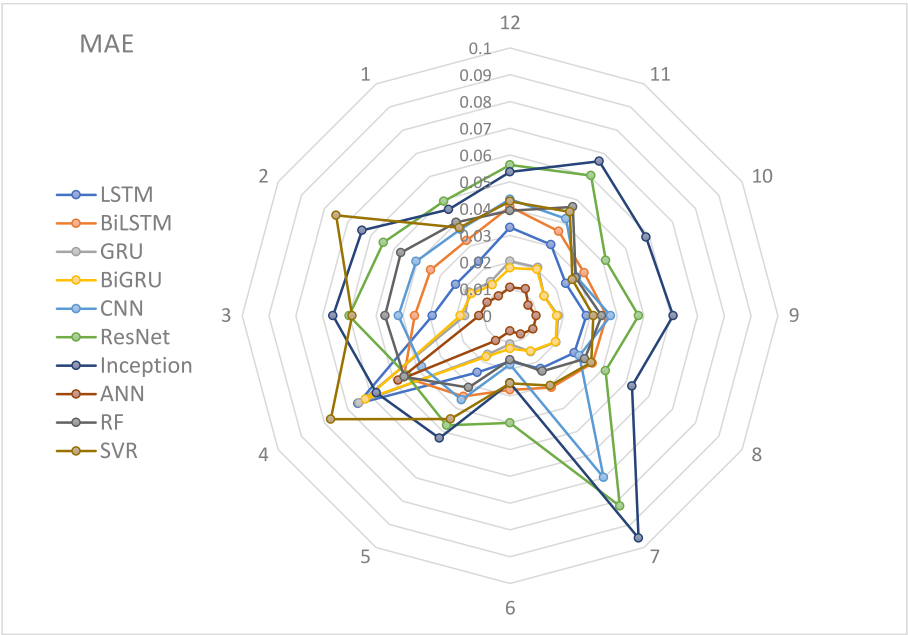

Fig. 17. Monthly variation of MAE for the developed models (3 h ahead).

- **Including further meteorological parameters** such as ambient temperature, relative humidity, wind speed, and atmospheric pressure may improve model accuracy by accounting for key environmental factors that influence PV system behavior.
- **Implementing the forecasting algorithm within a Smart Monitoring Device (SMD)** would provide a portable, real-time, and user-friendly tool for monitoring PV power generation. Such a device would be particularly valuable for the Djelfa PV power plant, especially in the context of grid integration and operational management.
- **Deploying the Smart Monitoring Device in neighboring regions** of Djelfa and in residential environments can support the optimal utilization of rooftop PV systems. The device may also be used in newly installed PV systems with limited historical data, where transfer learning techniques could enable the forecasting model to adapt effectively to the new environment.
- **Applying the model in various geographic locations** beyond Djelfa is essential for assessing its generalizability and adaptability to diverse climatic and environmental conditions. This step is critical for verifying the scalability and practical relevance of the proposed forecasting framework.

Taken together, these recommendations offer a promising pathway for expanding the utility, robustness, and real-world deployment potential of PV forecasting models in support of broader renewable energy goals.

Funding declaration

No funding was received for conducting this study.

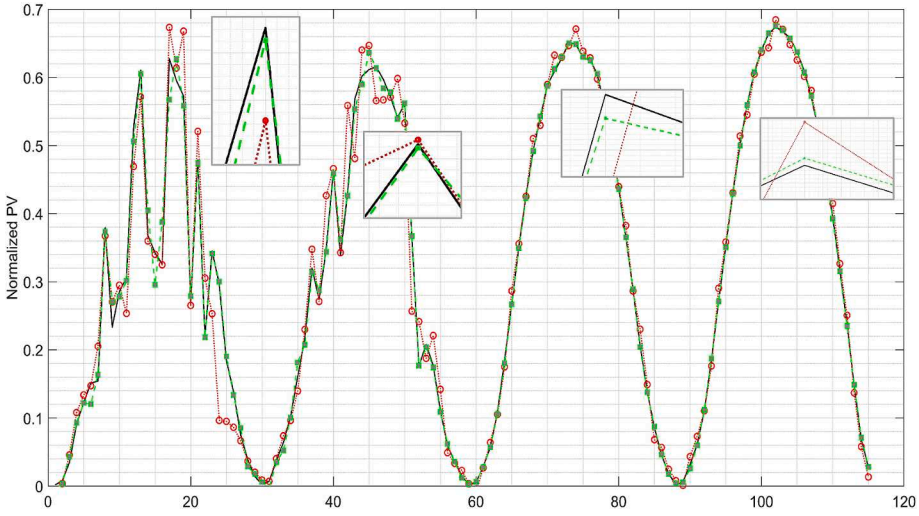

Fig. 18. Performance metrics for different weather conditions (30 min ahead).

CRediT authorship contribution statement

Ferial El Robrini: Writing – review & editing, Writing – original draft, Visualization, Validation, Software, Methodology, Investigation, Formal analysis, Conceptualization. **Badia Amrouche:** Supervision, Project administration. **Umit Cali:** Writing – review & editing, Writing – original draft, Supervision, Investigation, Funding acquisition, Conceptualization. **Taha Selim Ustun:** Writing – review & editing, Writing – original draft, Supervision, Investigation, Funding acquisition, Conceptualization.

Declaration of competing interest

The authors declare that they have no known competing financial interests or personal relationships that could have appeared to influence the work reported in this paper.

Data availability

Data will be made available on request.

References

[1] Farooq Z, Rahman A. Power Generation Control of Renewable Energy Based Hybrid Deregulated Power System. Energies 2022;15:517.
[2] Hussain I, Das DC, Sinha N, Latif A. Performance Assessment of an Islanded Hybrid Power System with Different Storage Combinations Using an FPA-Tuned Two-Degree-of-Freedom (2DOF) Controller. Energies 2020;13:5610.
[3] Abdolrasol MG, Ayob A, Mutlag AH. Optimal fuzzy logic controller based PSO for photovoltaic system. Energy Rep 2023;9:427–34.
[4] Ustun TS, Nakamura Y, Hashimoto J, Otani K. Performance analysis of PV panels based on different technologies after two years of outdoor exposure in Fukushima, Japan. Renew Energy 2019;136:159–78.
[5] Das A, Dawn S, Gope S. A Risk Curtailment Strategy for Solar PV-Battery Integrated Competitive Power System. Electronics 2022;11:1251.
[6] International Renewable Energy Agency (2024). *The energy transition in Africa: Opportunities for international collaboration with a focus on the G7*, Abu Dhabi.
[7] Largot S, et al. Experimental study on the effect of operational and environmental conditions on photovoltaic modules productivity in El-Oued region, algeria. Energy Convers Manage: X 2024. https://doi.org/10.1016/j.ecmx.2024.100655.
[8] Sepúlveda-Oviedo EH. A review of operational factors affecting photovoltaic system performance. Energy Convers Manage: X 2025. https://doi.org/10.1016/j.ecmx.2025.100942.
[9] Singh NK, Koley C, Gope S, Dawn S. An Economic Risk Analysis in Wind and Pumped Hydro Energy Storage Integrated Power System Using Meta-Heuristic Algorithm. Sustainability 2021;13:13542.
[10] Latif A, Hussain SMS, Das DC. Optimization of Two-Stage IPD-(1+I) Controllers for Frequency Regulation of Sustainable Energy Based Hybrid Microgrid Network. Electronics 2021;10:919.
[11] Al-Ali S, et al. A review of solar photovoltaic technologies: developments, challenges, and future perspectives. Energy Convers Manage: X 2025. https://doi.org/10.1016/j.ecmx.2025.101057.
[12] Das A, Dawn S, Gope S. A Strategy for System Risk Mitigation Using FACTS Devices in a Wind Incorporated Competitive Power System. Sustainability 2022;14:8069.
[13] Malik, H., Mishra, S., Sood, Y.R., Iqbal, A., Renewable Power for Sustainable Growth. ICRP 2023. Lecture Notes in Electrical Engineering, vol 1086. Springer, Singapore. https://doi.org/10.1007/978-981-99-6749-0_1.
[14] Alshahrani S, et al. Grid-Forming Converter and Stability Aspects of Renewable-Based Low-Inertia Power Networks: Modern Trends and Challenges. Arab J Sci Eng 2024. https://doi.org/10.1007/s13369-023-08399-z.
[15] Chakraborty MR, Dawn S, Saha PK, Basu JB. System Economy Improvement and Risk Shortening by Fuel Cell-UPFC Placement in a Wind-Combined System. Energies 2023;16:1621.
[16] Suresh Kumar B, et al. Prediction of Photovoltaic Power by ANN Based on Various Environmental Factors in India. Int J Photoenergy 2022. https://doi.org/10.1155/2022/4905980.
[17] Vanlalchhuanawmi C, Deb S, Onen A. Energy management strategies in distribution system integrating electric vehicle and battery energy storage system: A review. Energy Storage 2024;6(5):e682.
[18] Ali AO, et al. Advancements in photovoltaic technology: A comprehensive review of recent advances and future prospects. Energy Convers Manage: X 2025. https://doi.org/10.1016/j.ecmx.2025.100952.
[19] Meliani M, et al. Energy management in the smart grid: State-of-the-art and future trends. Int J Eng Bus Manage 2021. https://doi.org/10.1177/18479790211032920.
[20] Raza MQ, et al. On recent advances in PV output power forecast. Sol Energy 2016. https://doi.org/10.1016/j.solener.2016.06.073.
[21] Shab, G. (2022). Prévision multi-horizon de l'éclairement global horizontal pour la gestion intelligente du réseau électrique de distribution en région Occitanie.
[22] Shaik F, et al. Effect of various parameters on the performance of solar PV power plant: a review and the experimental study. Sustainable Energy Res 2023. https://doi.org/10.1186/s40807-023-00076-x.
[23] Rahimi N, et al. A Comprehensive Review on Ensemble Solar Power Forecasting Algorithms. J Electr Eng Technol 2023. https://doi.org/10.1007/s42835-023-01378-2.
[24] Diagne M, et al. Review of solar irradiance forecasting methods and a proposition for small-scale insular grids. Renew Sustain Energy Rev 2013. https://doi.org/10.1016/j.rser.2013.06.042.
[25] Antonanzas J, et al. Review of photovoltaic power forecasting. Sol Energy 2016. https://doi.org/10.1016/j.solener.2016.06.069.
[26] Akhter MN, et al. Review on forecasting of photovoltaic power generation based on machine learning and metaheuristic techniques. IET Renew Power Gener 2019. https://doi.org/10.1049/iet-rpg.2018.5649.
[27] Ahmed R, et al. A review and evaluation of the state-of-the-art in PV solar power forecasting: Techniques and optimization. Renew Sustain Energy Rev 2020. https://doi.org/10.1016/j.rser.2020.109792.
[28] Álvarez-Alvarado JM, et al. Hybrid techniques to predict solar radiation using support vector machine and search optimization algorithms: A review. Applied Sciences (Switzerland) 2021. https://doi.org/10.3390/app11031044.
[29] ElRobrini F, et al. Federated learning and non-federated learning based power forecasting of photovoltaic/wind power energy systems: A systematic review. Energy AI 2024. https://doi.org/10.1016/j.egyai.2024.100438.
[30] Raza MQ, et al. On recent advances in PV output power forecast. Sol Energy 2016. https://doi.org/10.1016/j.solener.2016.06.073.

[31] Yang D. Making reference solar forecasts with climatology, persistence, and their optimal convex combination. Sol Energy 2019. https://doi.org/10.1016/j.solener.2019.10.006.

[32] Ssekulima EB, et al. Wind speed and solar irradiance forecasting techniques for enhanced renewable energy integration with the grid: A review. IET Renew Power Gener 2016. https://doi.org/10.1049/iet-rpg.2015.0477.

[33] Das UK, et al. Forecasting of photovoltaic power generation and model optimization: A review. Renew Sustain Energy Rev 2018. https://doi.org/10.1016/j.rser.2017.08.017.

[34] Pandžić, F. *et al.* (2024). Cloud Effects on Photovoltaic Power Forecasting: Initial Analysis of a Single Power Plant Based on Satellite Images and Weather Forecasts, pp. 3–11.

[35] Cryer, J.D. and Chan, K.-S.Springer Texts in Statistics Time Series Analysis With Applications in R Second Edition.

[36] Kushwaha V, Pindoriya NM. A SARIMA-RVFL hybrid model assisted by wavelet decomposition for very short-term solar PV power generation forecast. Renew Energy 2019. https://doi.org/10.1016/j.renene.2019.03.020.

[37] Farsi M, et al. Parallel genetic algorithms for optimizing the SARIMA model for better forecasting of the NCDC weather data. Alex Eng J 2021. https://doi.org/10.1016/j.aej.2020.10.052.

[38] Huang J, et al. Forecasting solar radiation on an hourly time scale using a Coupled AutoRegressive and Dynamical System (CARDS) model. Sol Energy 2013. https://doi.org/10.1016/j.solener.2012.10.012.

[39] Dahmani K, et al. Estimation of 5-min time-step data of tilted solar global irradiation using ANN (Artificial Neural Network) model. Energy 2014. https://doi.org/10.1016/j.energy.2014.04.011.

[40] Maamar, L. *et al.* (2014). Prediction and extrapolation of global solar irradiation on tilted surfaces from horizontal ones using an artificial neural network. *3rd International Symposium on Environment Friendly Energies and Applications, EFEA 2014*. https://doi.org/10.1109/EFEA.2014.7059998.

[41] Benkaciali S, et al. Evaluation of the global solar irradiation from the artificial neural network technique. Revue des Energies 2016. Renouvelables.

[42] Khelifi R, et al. Multi-step-ahead forecasting of daily solar radiation components in the Saharan climate. Int J Ambient Energy 2020. https://doi.org/10.1080/01430750.2018.1490349.

[43] Amrouche B, Le Pivert X. Artificial neural network based daily local forecasting for global solar radiation. Appl Energy 2014. https://doi.org/10.1016/j.apenergy.2014.05.055.

[44] Yarar N, et al. Artificial neural networks based harmonics estimation for real university microgrids using hourly solar irradiation and temperature data. Energy Nexus 2023;9:100172.

[45] Guermoui M, Rabehi A. Soft computing for solar radiation potential assessment in Algeria. Int J Ambient Energy 2020. https://doi.org/10.1080/01430750.2018.1517686.

[46] Guermoui M, et al. Support vector regression methodology for estimating global solar radiation in Algeria. European Physical Journal Plus 2018. https://doi.org/10.1140/epjp/i2018-11845-y.

[47] Guermoui M, et al. New temperature-based predicting model for global solar radiation using support vector regression. Int J Ambient Energy 2022. https://doi.org/10.1080/01430750.2019.1708792.

[48] Hassan MA, et al. Ultra-short-term exogenous forecasting of photovoltaic power production using genetically optimized non-linear auto-regressive recurrent neural networks. Renew Energy 2021. https://doi.org/10.1016/j.renene.2021.02.103.

[49] Takilalte, A. *et al.* (2022). Forecasting global solar irradiance for various resolutions using time series models - case study: Algeria. *Energy Sources, Part A: Recovery, Utilization and Environmental Effects*. https://doi.org/10.1080/15567036.2019.1649756.

[50] Rabehi A, et al. Hybrid models for global solar radiation prediction: a case study. Int J Ambient Energy 2020. https://doi.org/10.1080/01430750.2018.1443498.

[51] Benmouiza K, Cheknane A. Forecasting hourly global solar radiation using hybrid k-means and nonlinear autoregressive neural network models. Energ Conver Manage 2013. https://doi.org/10.1016/j.enconman.2013.07.003.

[52] Benmouiza K, Cheknane A. Clustered ANFIS network using fuzzy c-means, subtractive clustering, and grid partitioning for hourly solar radiation forecasting. Theor Appl Climatol 2019. https://doi.org/10.1007/s00704-018-2576-4.

[53] El Bourakadi D, et al. A novel solar power prediction model based on stacked BiLSTM deep learning and improved extreme learning machine. International Journal of Information Technology (Singapore) 2023. https://doi.org/10.1007/s41870-022-01118-1.

[54] Guermoui M, et al. An analysis of case studies for advancing photovoltaic power forecasting through multi-scale fusion techniques. Sci Rep 2024. https://doi.org/10.1038/s41598-024-57398-z.

[55] Guermoui M, et al. A Novel Hybrid Model for Solar Radiation Forecasting Using Support Vector Machine and Bee Colony Optimization Algorithm: Review and Case Study. Journal of Solar Energy Engineering, Transactions of the ASME. 2021. https://doi.org/10.1115/1.4047852.

[56] Bouchouicha K, et al. Comparison of artificial intelligence and empirical models for energy production estimation of 20 MWp solar photovoltaic plant at the Saharan Medium of Algeria. Int J Energy Sect Manage 2021. https://doi.org/10.1108/IJESM-12-2019-0017.

[57] El Robrini F, Amrouche B. Exploring Forecasting and Prediction Processes for Decision-Making to Promote the Photovoltaic Energy Integration into the Grid : Mini Review. International Conference on Decision Aid Sciences and Applications 2023. https://doi.org/10.1109/DASA59624.2023.10286623.

[58] Geng, D. *et al.* (2023). A hybrid photovoltaic/wind power prediction model based on Time2Vec, WDCNN and BiLSTM. *Energy Conversion and Management*. https://doi.org/10.1016/j.enconman.2023.117342.

[59] Feroz Mirza A, et al. Hybrid Inception-embedded deep neural network ResNet for short and medium-term PV-Wind forecasting. Energ Conver Manage 2023. https://doi.org/10.1016/j.enconman.2023.117574.

[60] Wang F, et al. A day-ahead PV power forecasting method based on LSTM-RNN model and time correlation modification under partial daily pattern prediction framework. Energ Conver Manage 2020. https://doi.org/10.1016/j.enconman.2020.112766.

[61] Mansoor M, et al. Hybrid forecasting models for wind-PV systems in diverse geographical locations: Performance and power potential analysis. Energ Conver Manage 2023. https://doi.org/10.1016/j.enconman.2023.117080.

[62] Hassan MA, et al. Ultra-short-term exogenous forecasting of photovoltaic power production using genetically optimized non-linear auto-regressive recurrent neural networks. Renew Energy 2021. https://doi.org/10.1016/j.renene.2021.02.103.

[63] Keddouda A, et al. Solar photovoltaic power prediction using artificial neural network and multiple regression considering ambient and operating conditions. Energ Conver Manage 2023. https://doi.org/10.1016/j.enconman.2023.117186.

[64] Khelifi R, et al. Short-Term PV Power Forecasting Using a Hybrid TVF-EMD-ELM Strategy. Int Trans Electr Energy Syst 2023. https://doi.org/10.1155/2023/6413716.

[65] Guermoui M, et al. Forecasting intra-hour variance of photovoltaic power using a new integrated model. Energy Conversion and Management 2021. https://doi.org/10.1016/j.enconman.2021.114569.

[66] Ziane A, et al. Photovoltaic output power performance assessment and forecasting: Impact of meteorological variables. Sol Energy 2021. https://doi.org/10.1016/j.solener.2021.04.004.

[67] Dairi A, et al. Short-term forecasting of photovoltaic solar power production using variational auto-encoder driven deep learning approach. Applied Sciences (Switzerland) 2020. https://doi.org/10.3390/app10238400.

[68] https://www.meteo.dz/home.

[69] World Meteorological Organizationhttps://worldweather.wmo.int/en/city.html?cityId=1438.

[70] Weather Atlas (2024). https://www.weather-atlas.com/en/algeria/djelfa-climate.

[71] El Robrini F, Amrouche B. Daily Forecasting of Photovoltaic Power Generation with Multi Technological data Using Enhanced Long Short-Term Memory Networks . *Journal of Physical & Chemical.* Research 2024.

[72] El Robrini F, Amrouche B. Three Hour Ahead PV Power Forecasting with Bidirectional Recurrent Networks: Insights into Monthly Variability. *Journal of Renewable.* Energies 2025.

[73] Agga, A. *et al.* (2021). Short-term self consumption PV plant power production forecasts based on hybrid CNN-LSTM, ConvLSTM models. *Renewable Energy*. https://doi.org/10.1016/j.renene.2021.05.095.

[74] Cao Y, et al. Multi-timescale photovoltaic power forecasting using an improved Stacking ensemble algorithm based LSTM-Informer model. Energy 2023. https://doi.org/10.1016/j.energy.2023.128669.

[75] Liu Q, et al. A cloud-based Bi-directional LSTM approach to grid-connected solar PV energy forecasting for multi-energy systems. Sustainable Computing: Informatics and Systems. 2023. https://doi.org/10.1016/j.suscom.2023.100892.

[76] Dhaked DK, et al. Power output forecasting of solar photovoltaic plant using LSTM. Green Energy Intell Transp 2023. https://doi.org/10.1016/j.geits.2023.100113.

[77] Al-Ja'afreh MAA, et al. An enhanced CNN-LSTM based multi-stage framework for PV and load short-term forecasting: DSO scenarios. Energy Rep 2023. https://doi.org/10.1016/j.egyr.2023.08.003.

[78] Sadeghi D, et al. Improving PV power plant forecast accuracy: A hybrid deep learning approach compared across short, medium, and long-term horizons. Renewable Energy Focus 2023. https://doi.org/10.1016/j.ref.2023.04.010.

[79] Mamdouh M, et al. Improving flight delays prediction by developing attention-based bidirectional LSTM network. Expert Syst Appl 2024. https://doi.org/10.1016/j.eswa.2023.121747.

[80] Wu F, et al. An improved convolutional neural network-bidirectional gated recurrent unit algorithm for robust state of charge and state of energy estimation of new energy vehicles of lithium-ion batteries. J Storage Mater 2024. https://doi.org/10.1016/j.est.2024.110574.

[81] Taskin SG, et al. Detection of Turkish Fake News in Twitter with Machine Learning Algorithms. Arab J Sci Eng 2022. https://doi.org/10.1007/s13369-021-06223-0.

[82] Yu, H. and Kim, S. (2012). SVM tutorial-classification, regression and ranking, in *Handbook of Natural Computing*, vol. 1–4, Springer Berlin Heidelberg, pp. 479–506.

[83] Lateko AAH, et al. Short-Term PV Power Forecasting Using a Regression-Based Ensemble Method. Energies 2022. https://doi.org/10.3390/en15114171.

[84] Zemouri, N. and Bouzgou, H. (2018). Ensemble of Support Vector Methods to Estimate Global Solar Radiation in Algeria, in *Lecture Notes in Networks and Systems*, vol. 35, Springer, pp. 155–163.

[85] Xiao B, et al. Gray-Related Support Vector Machine Optimization Strategy and Its Implementation in Forecasting Photovoltaic Output Power. Int J Photoenergy 2022. https://doi.org/10.1155/2022/3625541.

[86] Borup D, et al. Targeting predictors in random forest regression. Int J Forecast 2023. https://doi.org/10.1016/j.ijforecast.2022.02.010.

[87] Ait tchakoucht T, et al. Random forest with feature selection and K-fold cross validation for predicting the electrical and thermal efficiencies of air based

photovoltaic-thermal systems. Energy Rep 2024. https://doi.org/10.1016/j.egyr.2024.07.002.
[88] Bueno-Barrachina J-M, et al. Inception 1D-convolutional neural network for accurate prediction of electrical insulator leakage current from environmental data during its normal operation using long-term recording. Eng Appl Artif Intel 2023. https://doi.org/10.1016/j.engappai.2022.105799.
[89] Kiranyaz S, et al. 1D convolutional neural networks and applications: A survey. Mech Syst Sig Process 2021. https://doi.org/10.1016/j.ymssp.2020.107398.
[90] Bueno-Barrachina J-M, et al. Inception 1D-convolutional neural network for accurate prediction of electrical insulator leakage current from environmental data during its normal operation using long-term recording. Eng Appl Artif Intell 2023. https://doi.org/10.1016/j.engappai.2022.105799.
[91] Yu J, Zhou X. One-Dimensional Residual Convolutional Autoencoder Based Feature Learning for Gearbox Fault Diagnosis. IEEE Trans Ind Inf 2020. https://doi.org/10.1109/TII.2020.2966326.
[92] Miraftabzadeh SM, Longo M. High-resolution PV power prediction model based on the deep learning and attention mechanism. Sustainable Energy Grids Networks 2023. https://doi.org/10.1016/j.segan.2023.101025.
[93] Li Y, Yang C. Multi time scale inception-time network for soft sensor of blast furnace ironmaking process. J Process Control 2022. https://doi.org/10.1016/j.jprocont.2022.08.003.
[94] Zhang K, et al. Multi-step forecast of PM2.5 and PM10 concentrations using convolutional neural network integrated with spatial–temporal attention and residual learning. Environ Int 2023. https://doi.org/10.1016/j.envint.2022.107691.
[95] Yin L, Zhao M. Inception-embedded attention memory fully-connected network for short-term wind power prediction. Appl Soft Comput 2023. https://doi.org/10.1016/j.asoc.2023.110279.
[96] Neshat M, et al. Short-term solar radiation forecasting using hybrid deep residual learning and gated LSTM recurrent network with differential covariance matrix adaptation evolution strategy. Energy 2023. https://doi.org/10.1016/j.energy.2023.127701.
[97] He K, et al. Deep Residual Learning for Image Recognition. In: 2016 IEEE Conference on Computer Vision and Pattern Recognition (CVPR); 2016. https://doi.org/10.1109/CVPR.2016.90.
[98] Yildiz C, et al. An improved residual-based convolutional neural network for very short-term wind power forecasting. Energ Conver Manage 2021. https://doi.org/10.1016/j.enconman.2020.113731.
[99] Liu R, et al. Multiscale Kernel Based Residual Convolutional Neural Network for Motor Fault Diagnosis under Nonstationary Conditions. IEEE Trans Ind Inf 2020. https://doi.org/10.1109/TII.2019.2941868.
[100] Chen Q, et al. A novel trilinear deep residual network with self-adaptive Dropout method for short-term load forecasting. Expert Syst Appl 2021. https://doi.org/10.1016/j.eswa.2021.115272.
[101] Han Y, et al. Ultra-short-term wind power interval prediction based on hybrid temporal inception convolutional network model. Electr Pow Syst Res 2023. https://doi.org/10.1016/j.epsr.2023.109159.
[102] Ferkous K, et al. A novel learning approach for short-term photovoltaic power forecasting - A review and case studies. Eng Appl Artif Intel 2024. https://doi.org/10.1016/j.engappai.2024.108502.
[103] Dragomiretskiy K, Zosso D. Variational Mode Decomposition. IEEE Trans Signal Process 2014. https://doi.org/10.1109/TSP.2013.2288675.
[104] Taye, M.M. (2023). Theoretical Understanding of Convolutional Neural Network: Concepts, Architectures, Applications, Future Directions. *Computation*. https://doi.org/10.3390/computation11030052.
[105] Liu Y, et al. Non-ferrous metals price forecasting based on variational mode decomposition and LSTM network. Knowl-Based Syst 2020. https://doi.org/10.1016/j.knosys.2019.105006.
[106] Ali M, et al. Variational mode decomposition based random forest model for solar radiation forecasting: New emerging machine learning technology. Energy Rep 2021. https://doi.org/10.1016/j.egyr.2021.09.113.
[107] Sivakumar M, et al. Nine novel ensemble models for solar radiation forecasting in Indian cities based on VMD and DWT integration with the machine and deep learning algorithms. Comput Electr Eng 2023. https://doi.org/10.1016/j.compeleceng.2023.108691.
[108] Piotrowski P, et al. Evaluation Metrics for Wind Power Forecasts: A Comprehensive Review and Statistical Analysis of Errors. Energies 2022. https://doi.org/10.3390/en15249657.
[109] Hu H, et al. Forecasting energy consumption and wind power generation using deep echo state network. Renew Energy 2020. https://doi.org/10.1016/j.renene.2020.03.042.
[110] Shen Y, et al. Wind Power Forecasting Using Multi-Objective Evolutionary Algorithms for Wavelet Neural Network-Optimized Prediction Intervals. Appl Sci 2018. https://doi.org/10.3390/app8020185.
[111] Wang L, et al. Effective electricity energy consumption forecasting using echo state network improved by differential evolution algorithm. Energy 2018. https://doi.org/10.1016/j.energy.2018.04.078.
[112] Harrison B, Bales R. Skill Assessment of Water Supply Outlooks in the Colorado River Basin. Hydrology 2015. https://doi.org/10.3390/hydrology2030112.
[113] El Robrini F, Amrouche B. Support Vector Regression for Predicting Intra-day Photovoltaic Generation in Algeria. International Conference on Electronics, Energy, and Measurement. 2023. https://doi.org/10.1109/IC2EM59347.2023.10419659.
[114] Krichen M. Convolutional Neural Networks: A Survey. Computers 2023. https://doi.org/10.3390/computers12080151.
[115] Lodhi E, et al. Enhancing microgrid forecasting accuracy with SAQ-MTCLSTM: A self-adjusting quantized multi-task ConvLSTM for optimized solar power and load demand predictions. Energy Convers Manage: X 2024. https://doi.org/10.1016/j.ecmx.2024.100767.
[116] Li Y, et al. Short-term PV power prediction based on meteorological similarity days and SSA-BiLSTM. Syst Soft Comput 2024. https://doi.org/10.1016/j.sasc.2024.200084.
[117] Zafar MH, et al. DeepTimeNet: A novel architecture for precise surface temperature estimation of lithium-ion batteries across diverse ambient conditions. Case Stud Therm Eng 2024. https://doi.org/10.1016/j.csite.2024.105002.
[118] Bian M, et al. Short-Term Load Forecastiong Based on Residual Graph Convolutional Neural Network. In: 2023 International Conference on Power System Technology (PowerCon); 2023. https://doi.org/10.1109/PowerCon58120.2023.10331583.
[119] Zafar MH, et al. Hierarchical Recurrent-Inception Residual Transformer (HRIRT) for Multidimensional Hand Force Estimation Using Force Myography Sensor. IEEE Sens Lett 2024. https://doi.org/10.1109/LSENS.2024.3431433.
[120] Hosseini Dehshiri SS, Firoozabadi B. Robust analysis of photovoltaic plants: A framework based on prediction uncertainties by machine learning. Energy Convers Manage: X 2025. https://doi.org/10.1016/j.ecmx.2025.100912.
[121] Khelifi R, et al. Short-Term PV Power Forecasting Using a Hybrid TVF-EMD-ELM Strategy. Int Trans Electr Energy Syst 2023. https://doi.org/10.1155/2023/6413716.